Diversity and Evolution of Frog Visual Opsins: Spectral Tuning and Adaptation to Distinct Light Environments

Ryan K. Schott [1,2,*] Matthew K. Fujita,[3] Jeffrey W. Streicher,[4] David J. Gower [4] Kate N. Thomas,[3,4] Ellis R. Loew,[5] Abraham G. Bamba Kaya,[6] Gabriela B. Bittencourt-Silva,[4] C. Guillherme Becker,[7] Diego Cisneros-Heredia,[8] Simon Clulow,[9] Mateo Davila,[8] Thomas J. Firneno Jr,[10] Célio F.B. Haddad,[11] Sunita Janssenswillen,[12] Jim Labisko,[4,13,14] Simon T. Maddock,[4,14,15] Michael Mahony,[16] Renato A. Martins,[17] Christopher J. Michaels,[18] Nicola J. Mitchell,[19] Daniel M. Portik [20] Ivan Prates [21] Kim Roelants,[12] Corey Roelke,[3] Elie Tobi,[22] Maya Woolfolk,[2,23] and Rayna C. Bell [2,20,*]

[1]Department of Biology and Centre for Vision Research, York University, Toronto, Ontario, Canada

[2]Department of Vertebrate Zoology, National Museum of Natural History, Smithsonian Institution, Washington, DC, USA

[3]Department of Biology, Amphibian and Reptile Diversity Research Center, The University of Texas at Arlington, Arlington, TX, USA

[4]Natural History Museum, London, UK

[5]Department of Biomedical Sciences, Cornell University College of Veterinary Medicine, Ithaca, NY, USA

[6]Institute de Recherches Agronomiques et Forestières, Libreville, Gabon

[7]Department of Biology and One Health Microbiome Center, Center for Infectious Disease Dynamics, The Huck Institutes of the Life Sciences, The Pennsylvania State University, University Park, PA, USA

[8]Laboratorio de Zoología Terrestre, Instituto de Biodiversidad Tropical IBIOTROP, Colegio de Ciencias Biológicas y Ambientales, Universidad San Francisco de Quito USFQ, Quito, Ecuador

[9]Centre for Conservation Ecology and Genomics, Institute for Applied Ecology, University of Canberra, Bruce, ACT, Australia

[10]Department of Biological Sciences, University of Denver, Denver, USA

[11]Department of Biodiversity and Center of Aquaculture—CAUNESP, I.B., São Paulo State University, Rio Claro, São Paulo, Brazil

[12]Amphibian Evolution Lab, Biology Department, Vrije Universiteit Brussel, Brussels, Belgium

[13]Centre for Biodiversity and Environment Research, Department of Genetics, Evolution and Environment, University College London, London, UK

[14]Island Biodiversity and Conservation Centre, University of Seychelles, Mahé, Seychelles

[15]School of Natural and Environmental Sciences, Newcastle University, Newcastle Upon Tyne, UK

[16]Department of Biological Sciences, The University of Newcastle, Newcastle 2308, Australia

[17]Programa de Pós-graduação em Conservação da Fauna, Universidade Federal de São Carlos, São Carlos, Brazil

[18]Independent Scholar, London, UK

[19]School of Biological Sciences, The University of Western Australia, Crawley, WA 6009, Australia

[20]Department of Herpetology, California Academy of Sciences, San Francisco, CA, USA

[21]Department of Biology, Lund University, Lund, Sweden

[22]Gabon Biodiversity Program, Center for Conservation and Sustainability, Smithsonian National Zoo and Conservation Biology Institute, Gamba, Gabon

[23]Department of Organismic and Evolutionary Biology, Museum of Comparative Zoology, Harvard University, Cambridge, MA, USA

*Corresponding authors: E-mails: schott@yorku.ca; rbell@calacademy.org.

Associate editor: Keith Crandall

Abstract

Visual systems adapt to different light environments through several avenues including optical changes to the eye and neurological changes in how light signals are processed and interpreted. Spectral sensitivity can evolve via changes to visual pigments housed in the retinal photoreceptors through gene duplication and loss, differential and coexpression, and sequence evolution. Frogs provide an excellent, yet understudied, system for visual evolution

Open Access

research due to their diversity of ecologies (including biphasic aquatic-terrestrial life cycles) that we hypothesize imposed different selective pressures leading to adaptive evolution of the visual system, notably the opsins that encode the protein component of the visual pigments responsible for the first step in visual perception. Here, we analyze the diversity and evolution of visual opsin genes from 93 new eye transcriptomes plus published data for a combined dataset spanning 122 frog species and 34 families. We find that most species express the four visual opsins previously identified in frogs but show evidence for gene loss in two lineages. Further, we present evidence of positive selection in three opsins and shifts in selective pressures associated with differences in habitat and life history, but not activity pattern. We identify substantial novel variation in the visual opsins and, using microspectrophotometry, find highly variable spectral sensitivities, expanding known ranges for all frog visual pigments. Mutations at spectral-tuning sites only partially account for this variation, suggesting that frogs have used tuning pathways that are unique among vertebrates. These results support the hypothesis of adaptive evolution in photoreceptor physiology across the frog tree of life in response to varying environmental and ecological factors and further our growing understanding of vertebrate visual evolution.

Key words: amphibia, codon-based selection models, sensory biology, vision research.

Introduction

Vision plays a key role in shaping complex animal behaviors including resource acquisition, predator avoidance, and mate choice (Cronin et al. 2014). Across the planet's diverse habitats, animal species contend with drastically different visual environments, which have resulted in the evolution of various visual systems (Land and Nilsson 2012). Adaptations to different visual environments can occur at multiple levels of the visual perception pathway but among the most impactful are adaptations in the visual opsin proteins that can directly modify light sensitivity, and how light signals are transmitted downstream, ultimately influencing other levels of visual perception (Davies et al. 2012).

Visual opsins are the protein component of the light-sensitive visual pigments that detect and respond to light signals. In vertebrates, visual opsins occur in the rod and cone photoreceptor cells of the retina, which are typically responsible for vision in dim and bright light, respectively. The last common ancestor of vertebrates had five distinct visual opsins (e.g. Davies et al. 2012): a rod-specific opsin, RH1, found in a single type of rod cell; and four cone opsins (LWS, RH2, SWS1, and SWS2), each present in a spectrally distinct class of cone (Fig. 1). The visual pigments formed by each of these different opsins absorb light maximally at different wavelengths (λ_{max}), and it is the different protein sequences (and resulting structural differences) among the five opsins that are largely responsible for these differences (Bowmaker 2008; Yokoyama 2008; Hagen et al. 2023). Although the spectral sensitivities of the rod and each of the four cone visual pigments are largely conserved, these can vary substantially among vertebrate groups due to interspecific variation in the opsin proteins (spectral tuning; Fig. 1).

An additional spectral-tuning mechanism in vertebrates involves the other component of visual pigments, the light-sensitive chromophore, which is covalently bound to the visual opsin protein to form a visual pigment. Most vertebrates exclusively use a vitamin A_1 derived chromophore (retinal, A_1), but some use a chromophore derived from vitamin A_2 (3,4-didehydroretinal, A_2) that

red-shifts and broadens the absorption spectra of the visual pigment relative to the A_1 form and lowers the photosensitivity (Bridges 1972; Corredor et al. 2022). Use of A_2 may be exclusive, shift through ontogeny, be present in a mixture with A_1, or be spatially distributed across the retina. A_2 is most often, but not exclusively, found in species inhabiting freshwater habitats in which the light environment is red shifted (Bridges 1972; Loew et al. 2002; Carleton et al. 2020; Corredor et al. 2022).

Adaptation in visual opsins has been found in many vertebrate groups, including both changes to spectral sensitivity (spectral tuning) and changes to other aspects of visual pigment function such as dark- and light-induced activation and decay rates (for simplicity, we hereafter refer to these collectively as kinetic rates). For example, differences in opsin selective constraint and the decay rate of the light-activated state were found among bat species with different habitat usage and feeding ecologies (Gutierrez et al. 2018a, 2018b). Similarly, in lemurs and birds, there is evidence for differences in opsin selective constraint, spectral tuning, and (in some cases) gene loss in species that inhabit closed versus open canopy habitats (Veilleux et al. 2013; Bloch et al. 2015). Shifts between diurnal and nocturnal activity patterns have been linked to positive selection and visual opsin gene loss in birds and snakes (Simões et al. 2016; Wu et al. 2016; Hauzman et al. 2017; Schott et al. 2018). Species that inhabit highly light-limited environments, such as fossorial mammals and deep-sea fishes, show patterns of gene loss and a relaxation of selective constraint on visual opsins and other visual genes (Emerling and Springer 2014; Partha et al. 2017; Lupše et al. 2021). Collectively, these studies highlight how differences in habitat and ecology can influence the evolution of vertebrate opsins, and vision more broadly.

Despite these advances, we still have very limited knowledge on the relationships between visual opsins and ecological diversity in a key vertebrate group: amphibians. Among them, frogs and toads (Anura—here collectively termed "frogs") are an especially diverse radiation, with ~7,600 extant species that encompass a diversity of behaviors and inhabit a wide variety of spectrally distinct
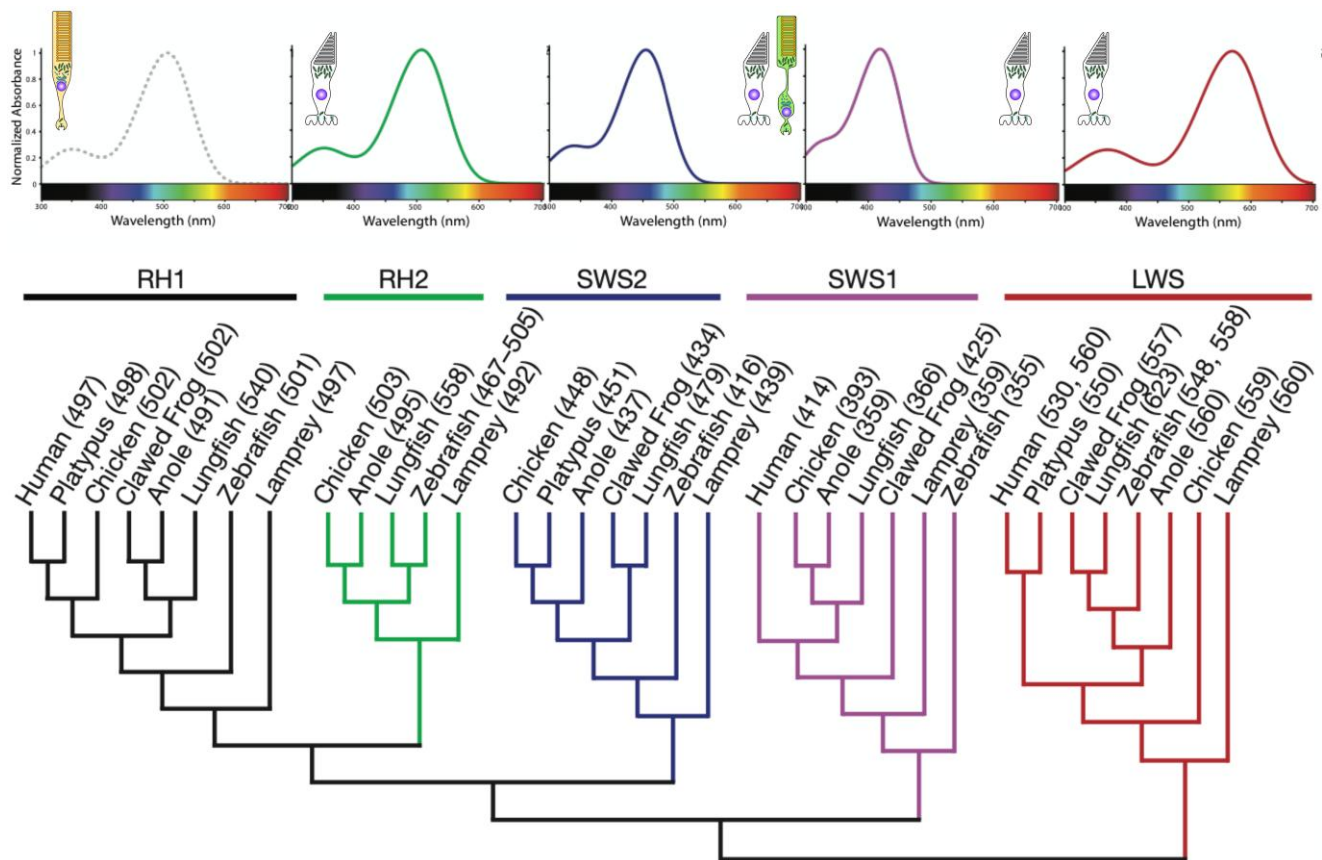
Fig. 1. The ancestor of vertebrates had five distinct visual opsins: a rod-specific opsin, RH1, found in a single type of rod cell; and four cone opsins (LWS, RH2, SWS1, and SWS2), each present in a spectrally distinct class of cone. Most amphibians have an additional photoreceptor cell type, the blue-sensitive rods (also referred to as "green rods"), which express a cone visual pigment (SWS2). The visual pigments formed by each of the different opsins absorb light maximally at different wavelengths (λ_{max}), as illustrated by the representative absorbance plots, and even minor changes to the protein sequences can shift the sensitivity of the visual pigment and impact other aspects of visual pigment function. Cladogram of visual opsin relationships adapted from Davies et al. (2012). Pigment absorbances (in parentheses, nm) were estimated from in vitro expression with the exception of lungfish, which was measured with microspectrophotometry (MSP). Values retrieved from the following references: human (Yokoyama 2008; Davies et al. 2012), platypus (Yokoyama 2008; Davies et al. 2012), chicken (measurements shown are for pigeon; Yokoyama 2008), clawed frog (Darden et al. 2003; Yokoyama 2008), anole (Yokoyama 2008), lungfish (Hart et al. 2008), zebrafish (Yokoyama 2008), and lamprey (Davies et al. 2012). Humans and zebrafish have two copies of LWS that differ in absorbance. Zebrafish have multiple copies of RH2 that differ in absorbance (minimum and maximum values shown).

environments from fossorial (e.g. subterranean) to aquatic (e.g. ponds and streams) and to arboreal (e.g. trees and other vegetation). Frogs are highly visual with the largest relative eye size among vertebrates (Thomas et al. 2020) and use their visual system for multiple tasks including prey detection and capture, predator avoidance, intraspecific signaling, and habitat selection (Ingle 1976; Hödl and Amézquita 2001). Most frogs are nocturnal, but some species are strictly diurnal (Anderson and Wiens 2017) and though many species have complex life cycles and inhabit different environments as larvae (tadpoles) than they do as adults, several independent lineages are direct developers that lack a larval stage and hatch from eggs as froglets. These differences in ecology, habitat, and life history have had considerable influence on the evolution of frog visual systems. Fossorial and aquatic frog species, for example, have significantly lower eye investment (lower allometric growth), whereas arboreal or climbing species have greater eye investment (Thomas et al. 2020). The

ocular media, specifically the presence or absence of UV-absorbing pigments in the lens, also varies across frog species (Yovanovich et al. 2019; Yovanovich et al. 2020). Lower UV light transmission levels are associated with diurnal and scansorial (climbing) frogs, suggesting a potential photoprotective and acuity increasing function (Thomas et al. 2022a). Frog lens shape and size also vary with ecology: aquatic and fossorial species maintain spherical, tadpole-like lenses after metamorphosis rather than undergoing an ontogenetic shift to a flatter lens, which is found in most other species (Mitra et al. 2022). These studies show that ecology, and in particular aquatic, fossorial, and scansorial lifestyles, have influenced evolution of the frog visual system, and suggest that the genes underlying this diversity are under strong selection.

At the level of photoreceptors and visual pigments, little is known about the diversity among frog species and how cell types and spectral sensitivities have evolved with respect to visual ecology. In general, frogs have up to two

types of rods (maximally green and blue sensitive) and up to six types of cones including maximally red, green, blue, and violet-sensitive single and double cones (for reviews, see Donner and Yovanovich 2020; Schott et al. 2022b). The green-sensitive rods (homologous with other vertebrate rods) express the rod opsin RH1 and absorb maximally (λ_{max}) in the range of 491 to 503 nm (Liebman and Entine 1968; Siddiqi et al. 2004; Robertson et al. 2022). The blue-sensitive rods (unique to amphibians) express a cone visual pigment (SWS2) and have λ_{max} in the range of 430 to 440 nm (Liebman and Entine 1968; Hisatomi et al. 1999; Ma et al. 2001; Darden et al. 2003; Govardovskii and Reuter 2014; Robertson et al. 2022). These rods have historically been called "green rods" in the literature due to their green color under a light microscope (conversely, the green-sensitive rods have often been referred to as "red rods"; Govardovskii and Reuter 2014). For clarity, we avoid this terminology because it obfuscates the typical convention of referring to visual pigments based on the color of light they maximally absorb (rather than reflect). We thus refer to this cell type as blue-sensitive, or SWS2, rods. This rod type has been lost in at least one diurnal species, the strawberry poison frog, *Oophaga pumilio* (Siddiqi et al. 2004). The red-sensitive single and double cones have LWS visual pigments with a λ_{max} of ~560 to 575 nm (Liebman and Entine 1968; Liebman 1972; Siddiqi et al. 2004; Robertson et al. 2022). The presence of the other cone types is variable among studied species and includes both single cones and the accessory members of double cones. The identity of the visual pigment (and corresponding opsins) in these cones is often unclear but includes SWS1 (λ_{max} 425 to 466 nm) and possibly RH1 (typically expressed exclusively in rods; λ_{max} 489 to 500 nm) and SWS2 (λ_{max} ~430 nm; Liebman and Entine 1968; Hárosi 1982; Koskelainen et al. 1994; Starace and Knox 1998; Hisatomi et al. 1999; Siddiqi et al. 2004; Schott et al. 2022b). In terms of chromophore usage, variation has been reported among different anuran lineages. For example, the fully aquatic clawed frog *Xenopus laevis* uses exclusively A_2 chromophore throughout its life cycle, whereas species with biphasic aquatic-terrestrial life cycles including ranid and hylid frogs typically use exclusively or primarily A_2 as tadpoles and transition to exclusively or primarily A_1 as adults (for reviews, see Bridges 1972; Schott et al. 2022a). These changes are thought to be adaptive for shifting spectral sensitivity toward the light spectra of terrestrial habitats from the red-shifted freshwater environments of most tadpoles (e.g. *Lithobates*; Schott et al. 2022a), although not all frogs have this ontogenetic shift (e.g. *Bufo*; Bridges 1972).

Despite limited sampling (33 species from 12 families), previous molecular analyses of the visual opsin genes in frogs found considerable variation in opsin sequences, including (i) at sites known to affect spectral sensitivity in other vertebrates and (ii) positive selection in two of the opsins (LWS and RH1) (Schott et al. 2022b). This suggests considerable, unappreciated variation in the visual system of frogs that requires further investigation with an improved representation of the phylogenetic and ecological diversity of the group. Here, we expand sampling of frog visual opsins by sequencing 93 whole eye transcriptomes from 82 species and extracting opsin sequences from published genomes, transcriptomes, and GenBank for a total of 122 species across 34 of the 56 currently recognized families. We scored these species for a set of six ecological traits, which we used to analyze patterns of sequence variation and shifts in selective pressures using codon models of molecular evolution. Based on the previous findings for morphological and spectral differences in frog visual systems (Thomas et al. 2020, 2022a, 2022b; Mitra et al. 2022), we hypothesized that visual opsins in aquatic and fossorial species are under relaxed selective constraint due to lower eye investment, while scansorial species show evidence of diversifying selection indicative of adaptive evolution related to their greater eye investment and potential coevolution with pigmented lenses. Further, based on evidence that the SWS2 opsin is differentially expressed in tadpole and juvenile leopard frogs, which suggests distinct usage across life stages (Schott et al. 2022a), we hypothesized that SWS2 in direct-developing species experienced a release of selective constraint. More broadly, we hypothesized that the wide diversity of light environments inhabited by frogs has favored distinct combinations of photoreceptor sensitivity across species resulting in opsin spectral tuning. To test this, we employed a comparative evolutionary framework to identify new, potentially functional, variation in visual opsin sequences, investigated possible instances of gene loss, and tested for evidence of positive selection. Finally, we used microspectrophotometry (MSP) to measure spectral absorption curves of individual photoreceptor cells to directly investigate differences in spectral sensitivity in a subset of our study species and to assess the potential functional consequences of the molecular changes we identified.

Results

Molecular Evolution of Frog Visual Opsins
Four Visual Opsin Genes Consistently Recovered From Frog Whole Eye Transcriptomes With Evidence for Loss in Two Lineages

Complete or partial coding sequences of four opsins—RH1, LWS, SWS1, and SWS2—were recovered from the eye transcriptomes of 82 species (93 transcriptomes total; supplementary file S1, Supplementary Material online). Additional coding sequences were extracted from available frog genomes and transcriptomes, and from GenBank, providing a dataset containing 122 species (Fig. 2; supplementary fig. S1, Supplementary Material online). Target genes were not recovered from all species, and some species were represented by multiple sequences. This resulted in 125 RH1, 118 LWS, 113 SWS1, and 113 SWS2 sequences in total (supplementary file S1, Supplementary Material online; Schott et al. 2024a).
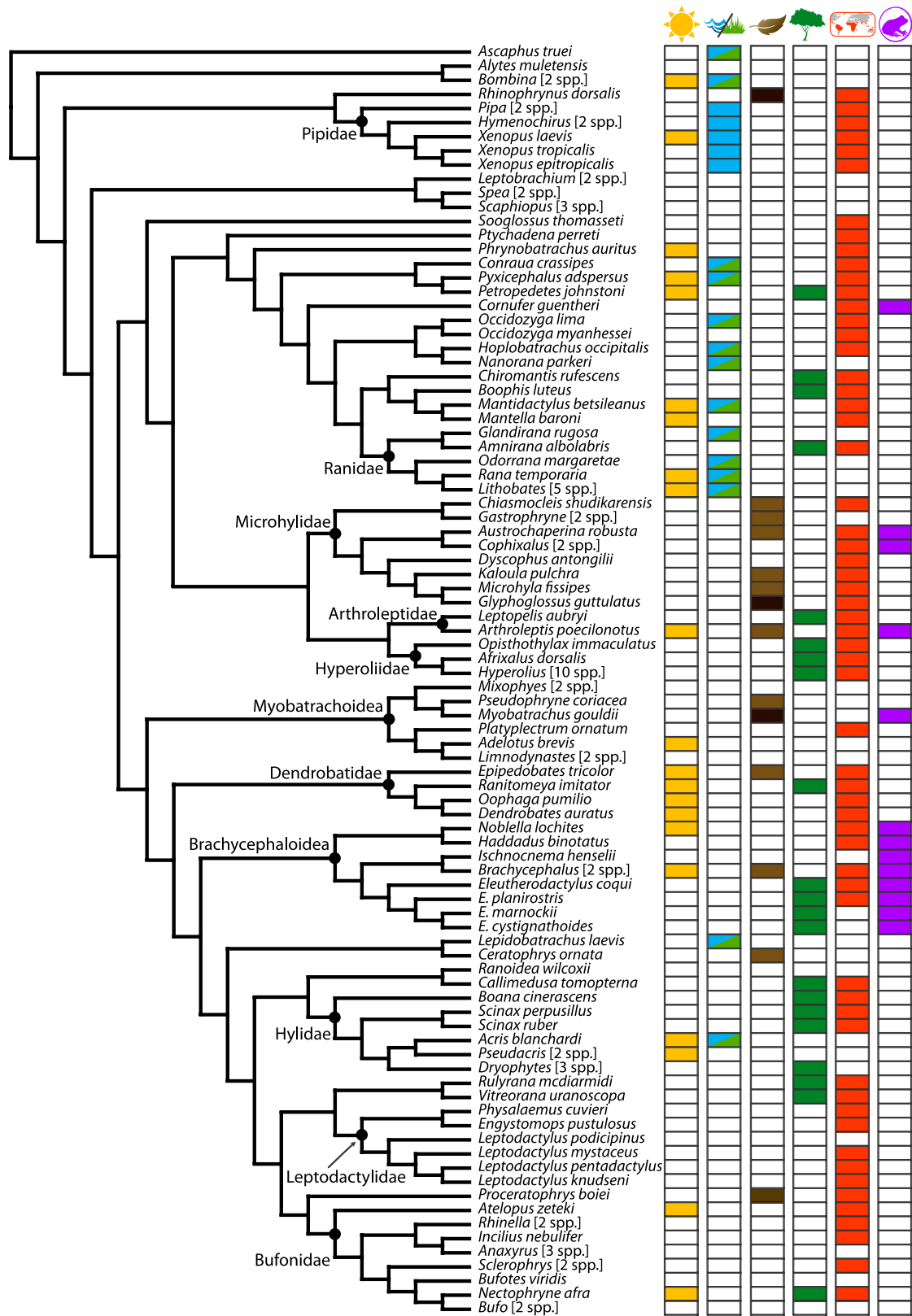
Fig. 2. Phylogenetic relationships and ecological trait assignments of the species included in the visual opsin datasets. Ecological trait classifications from left to right are diurnal activity (sun), aquatic or semiaquatic habit (waves/grass), secretive or fossorial activity (leaf), scansoriality (tree), tropical distribution (map), and direct development (frog egg). Fully aquatic species are denoted with a solid (blue) rectangle whereas semiaquatic species are split (blue/green). Fossorial species are denoted by a darker brown rectangle than subfossorial and other secretive species (e.g. leaf litter dwellers). Species within the same genus that share the same ecological traits have been collapsed to a single branch for display purposes, with the total number of sampled species shown in square brackets. Evolutionary relationships are based upon the phylogenetic hypothesis of Jetz and Pyron (2018). See supplementary fig. S1, Supplementary Material online for the full tree and supplementary file S1, Supplementary Material online for the complete ecological trait database (Supplementary Material online).

Previous studies have identified visual opsin gene duplication in *Xenopus laevis* both from the tetraploidization of the genome, which results in L and S homologs of most genes (Session et al. 2016), and a duplication of the *RH1* L homolog through what appears to be a tandem duplication (Batni et al. 1996; Feehan et al. 2017). We also identified two *LWS* homologs annotated on Xenbase (Fisher et al. 2023). Of these, the S homolog appears to be a pseudogene based on the presence of an internal stop codon and two frameshift deletions (supplementary fig. S2, Supplementary Material online; Schott et al. 2024a). *SWS1* and *SWS2* have only one annotated copy on Xenbase (the L and S homolog, respectively), but through BLAST searches of the *X. laevis* v10.1 assembly, we identified probable pseudogene fragments of the other homolog for each gene (supplementary figs. S3 and S4, Supplementary Material online; Schott et al. 2024a). We also found copies of *SWS1* on two scaffolds of the *Spea multiplicata* genome, one identified as a scaffold pertaining to chromosome 3 and another on an unidentified scaffold (scaff00005502). Because the *S. multiplicata* genome lacks a chromosome-level assembly and the two copies differ at only a single nucleotide, we consider it unlikely that this represents a gene duplication. In the *Hymenochirus boettgeri* genome three *LWS* variants were identified, and we found that these differ in the identity of the final exon (with one of the variants predicted to incorporate an additional exon), but evidence that these putative splice variants are expressed is lacking (supplementary fig. S2, Supplementary Material online; Schott et al. 2024a). Indeed, we found no evidence for these additional variants in the eye transcriptome of *H. curtipes*, which otherwise had an identical LWS coding sequence to *H. boettgeri*. We also identified three *H. boettgeri RH1* sequences through BLAST searches: one of these was the complete, annotated transcript; two others, found sequentially upstream on the opposite strand, were identical except for the presence of numerous short (1 to 3 nucleotide) insertions and deletions (Schott et al. 2024a). While it is possible these represent duplications that have been subsequently pseudogenized, the unusual pattern suggests they may be artefactual. The additional sequences noted above (except the duplications in *X. laevis*) were not included in further downstream analyses.

An *LWS* gene duplication was previously identified in the *Pyxicephalus adspersus* genome where one copy was found on each sex chromosome (W and Z; Schott et al 2022b). From our de novo assembly of the *P. adspersus* eye transcriptome, we were able to reconstruct two transcripts, one complete and one missing the first 109 nucleotides. The complete transcript was nearly identical to the W chromosome homolog, whereas the incomplete transcript was somewhat intermediate, with a mix of the differentiated W and Z residues (supplementary fig. S2, Supplementary Material online; Schott et al. 2024a). We considered this likely to result from incomplete de novo assembly due, at least in part, to the similarity between homologs. To determine whether both transcripts were

present in the transcriptome, we mapped the *P. adspersus* transcriptome reads to the genomic visual opsin coding sequences and extracted consensus sequences from the raw reads. Using this approach, we were able to recover complete coding sequences for both the W and Z homologs, with the Z homolog having nearly twice the average read depth (755 and 1,357 for W and Z, respectively; Schott et al. 2024a). The W and Z LWS homologs were included in the downstream analyses, but not the de novo assembled transcripts.

Genes with sequences that were not recovered from a single resource were generally not considered lost because their absence could be due to several causes other than gene loss, including incomplete sequencing or assembly coverage. In two cases, however, potential losses were corroborated by the absence of specific opsin gene sequences in multiple species within the same phylogenetic group. Specifically, all four species of Dendrobatidae (dart frogs) in our dataset lacked *SWS2*. This includes absence from eye transcriptomes of two specimens of *Dendrobates auratus* and one specimen of *Epipedobates tricolor* and from whole genome assemblies of *Oophaga pumilio* and *Ranitomeya imitator* (Rogers et al. 2018; Stuckert et al. 2021). Short fragments of sequences identified via BLAST as *SWS2* were found for both *O. pumilio* (86 bp, with an internal stop codon) and *R. imitator* (111 bp). Identification was confirmed by independently adding these fragments into the *SWS2* alignment, trimming to the fragment region, and inferring ML phylogenetic gene trees with PhyML (supplementary figs. S5 and S6, Supplementary Material online). This evidence across four genera suggests that all dendrobatids may have lost functional copies of the *SWS2* opsin gene. We also found that eye transcriptomes of arthroleptids in our dataset (*Arthroleptis poecilonotus* and *Leptopelis aubryi*) lack the *SWS1* gene. Unfortunately, no genome sequences for this family are currently available to further support the hypothesis of gene loss.

Evidence for Site-specific Positive Selection in Three of the Four Frog Visual Opsin Genes Suggests Potential Functional Adaptation

Results from the species-tree and gene-tree topologies were concordant and do not change the interpretations of the results, indicating robustness to minor differences in topology. We present the results from the species-tree topology analyses here, but gene-tree topology results are available online (supplementary files S2 and S3 and S4, Supplementary Material online; Schott et al. 2024a). We found similar levels of average selective constraint among the four visual opsins with *SWS2* under the highest constraint (M0 $\omega = 0.096$), *SWS1* under the lowest (M0 $\omega = 0.113$), and *RH1* and *LWS* with intermediate values (M0 $\omega = 0.106$ and 0.105, respectively; Fig. 3). Using the PAML M2a and M8 models, as well as the HYPHY BUSTED model, we found statistically significant positive selection at a small proportion of sites in *RH1*, *LWS*, and *SWS2* (Fig. 3; supplementary table S1, Supplementary Material online,
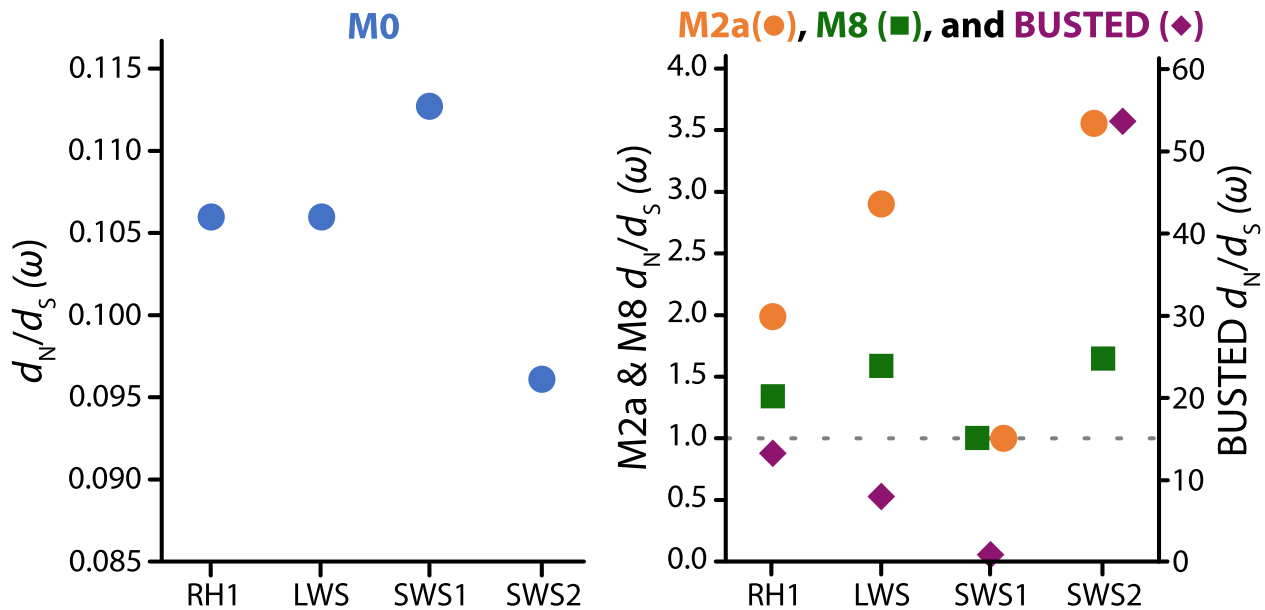
Fig. 3. Selective pressure on frog visual opsin genes estimated with PAML M0, M2a, and M8 models and the HYPHY model BUSTED. The M0 model estimates an average selective constraint across the entire gene coding sequence (left) and the M2a (circle), M8 (square), and BUSTED (diamond) models estimate selective pressure in multiple site classes including a class of sites that can have positive selection (right). The M2a, M8, and BUSTED graph depicts the ω value of the positively selected site class.

supplementary files S2 and S3, Supplementary Material online; Schott et al. 2024a). Six RH1 sites were inferred to be under positive selection with a BEB posterior probability of >80% with either the M2a or M8 models (39, 107, 169, 213, 270, and 290; site numbering is relative to bovine RH1 throughout). Although none have previously been identified to affect spectral tuning, most are close to known sites. FUBAR analysis identified five sites (87, 112, 133, 213, and 333; supplementary table S1, Supplementary Material online, supplementary file S4, Supplementary Material online), one of which overlapped with M2a$_{rel}$ and M8 (213). Five LWS sites were inferred to be under positive selection with posterior probability >80% using either the M2a or M8 models (49, 162, 164, 166, and 209), while FUBAR analysis identified three of the same sites (49, 162, and 166). Site 49 is a known spectral-tuning site in the RH2 and SWS1 opsins. In SWS2, two sites were inferred to be under positive selection by M2a or M8 (56, 282) and none with FUBAR. No evidence of positive selection in SWS1 was detected with the PAML models or BUSTED, but one site was identified with greater than 90% posterior probability using FUBAR (120).

Shifts in Selective Constraint on Visual Opsins are Associated With Changes in Habitat and Life History, But Not Activity Pattern

Shifts in selective constraint on the four visual opsin genes were tested using CmC with different ecological partitions (activity pattern, habitat, geographic distribution, and life history) as shown in Fig. 2. For each of the genes, we found a significant difference in selection pressures with at least one of the ecological partitions and, in each case, the best-fitting ecological partition was the same with either the

species- or gene-tree topology (supplementary file S2, Supplementary Material online; Schott et al. 2024a). To further investigate the basis for the selective differences identified with CmC, we performed additional analyses with the BUSTED and RELAX models to test for positive and relaxed selection, respectively, on the significant partitions (supplementary files S3 and S5, Supplementary Material online).

For *RH1*, we found the scansorial (arboreal) partition to be a significantly better fit than the null model (M2a$_{rel}$, LRT = 11.8, P = 0.0006), with scansorial species having higher ω (0.334) than nonscansorial species (0.222; Fig. 4). Two of the sites identified as being under positive selection in *RH1* (87, 133) were also inferred to be in the divergently selected site class with CmC with >80% posterior probability (supplementary file S2, Supplementary Material online). We found evidence for significant positive selection in the scansorial (arboreal) partition with BUSTED (LRT = 12.6, P = 0.0009) with stronger positive selection on scansorial species at a small proportion of sites (0.65%). We did not, however, find evidence for an overall relaxation of selective constraint on *RH1* in scansorial species with RELAX (K = 1.06 LRT = 0.30, P = 0.581). Evidence for a relaxation of selective constraint on aquatic and fossorial species was also not found (CmC: LRT = 0.362, P = 0.547. RELAX: K = 0.97, LRT = 0.00, P = 0.946).

For *LWS*, we found that two of the ecological partitions (aquatic and tropical) provided significantly better fits with CmC than with the null model, with the aquatic partition providing the best fit overall (LRT = 7.1, P = 0.0077; Fig. 4). Aquatic species had elevated ω relative to nonaquatic species (0.306 vs. 0.202), but we did not find overlap between sites inferred to be under positive selection and those
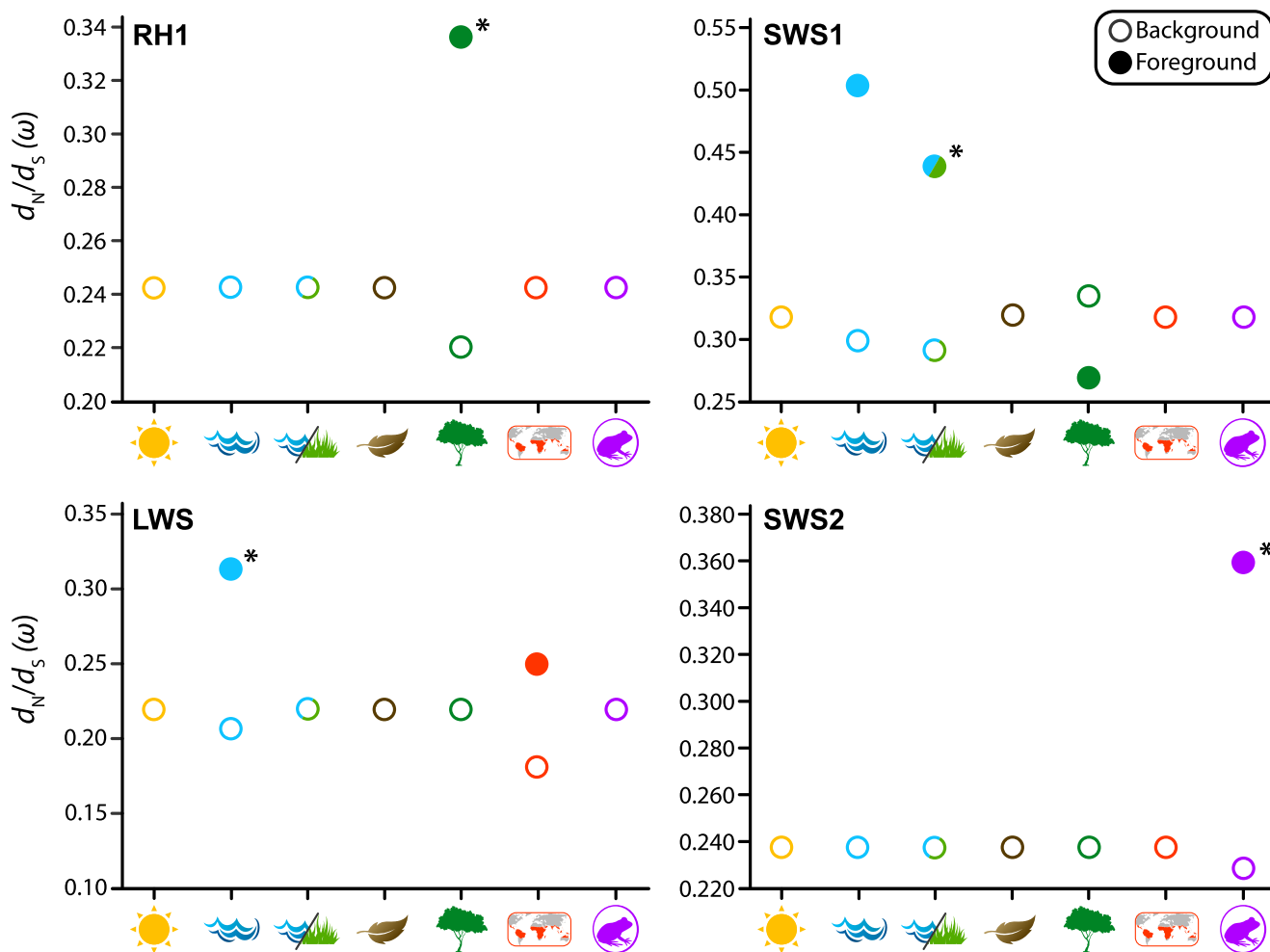
Fig. 4. Shifts in selective pressure on frog visual opsin genes associated with habitat, distribution, and life history. Selective pressure was estimated with PAML Clade model C (CmC) with separate models for each of the ecological partitions as shown in Fig. 2 (diurnal activity [sun], aquatic [waves], aquatic or semiaquatic [waves/grass], secretive or fossorial [leaf], scansoriality [tree], tropical distribution [map], and direct development [frog egg]). Ecological partitions with only open circles indicate that the null model (M2a) was a better fit than the CmC for that particular trait. Ecological partitions with both an open circle and a filled circle indicate that CmC was a better fit with open circles reflecting the background ω (frogs without the trait) and filled circles reflecting the foreground ω (frogs with the trait). Asterisks indicate the best-fitting partition for each opsin.

inferred to be divergently selected between aquatic and nonaquatic taxa (supplementary file S2, Supplementary Material online). We found no significant evidence for positive selection on the aquatic partition with BUSTED (LRT = 4.0, $P = 0.073$). The aquatic + semiaquatic partition, which was not significant with CmC, had significant evidence for positive selection (LRT = 8.2, $P = 0.008$), with the strength of positive selection on the aquatic + semiaquatic partition being lower ($\omega = 3.14$ vs. 10.20) but at a higher proportion of sites (2.47% vs. 0.52%) than in the non-(semi)aquatic species. RELAX analyses of the aquatic and aquatic + semiaquatic partitions were not significant (supplementary file S5, Supplementary Material online). There was, however, evidence for relaxed selection on aquatic and fossorial frogs ($K = 0.73$, LRT = 4.29, $P = 0.038$), and the aquatic + fossorial partition was also a better fit than the aquatic partition with CmC (LRT = 9.46, $P = 0.0021$), with elevated

ω in aquatic and fossorial species (0.306 vs. 0.202). We performed additional BUSTED analyses using this partition and found significant evidence for positive selection in aquatic and fossorial species (LRT = 8.2, $P = 0.009$) with lower ω in aquatic and fossorial species (3.42 vs.10.66) but at a higher proportion of sites (3.06% vs. 0.46%).

For *SWS1*, we found that three of the partitions showed a significantly better fit than the null model: scansorial, aquatic, and aquatic + semiaquatic (best-fitting partition; LRT = 18.23, $P < 0.000$; Fig. 4). Aquatic and semiaquatic species were estimated to have higher ω than other species (0.44 vs. 0.30). The single site identified as positively selected in SWS1 (120) was also inferred to be in the divergently selected site class (supplementary table S1, Supplementary Material online, supplementary file S2, Supplementary Material online). With BUSTED, we did not find evidence for positive selection on the aquatic +

semiaquatic partition ($P = 0.173$), but analysis of only the aquatic taxa found significant positive selection (LRT = 7.2, $P = 0.014$), with aquatic species having higher ω (5.39 vs. 1.56) at a similar number of sites (1.67% vs. 2.04%). Analyses with RELAX found significant evidence for relaxation of selective constraint on both the aquatic ($k = 0.63$, LRT = 17.70, $P < 0.000$) and the aquatic + semiaquatic partitions ($k = 0.62$, LRT = 31.89, $P < 0.000$), perhaps explaining the elevated ω found with CmC, but in contrast to the increased strength of positive selection in aquatic species identified with BUSTED. We also found evidence of relaxed selection on the aquatic + fossorial partition ($k = 0.79$, LRT = 14.06, $P < 0.000$).

Tests on *SWS2* revealed a single partition with a significantly better fit than the null model: life history (LRT = 7.80, $P = 0.005$), with direct-developing species having higher ω than other species (0.36 vs. 0.23). The two positively selected sites identified in *SWS2* (56 and 282) were not inferred to be in the divergently selected site class. There was no evidence for positive selection with the direct-development partition using BUSTED ($P = 0.069$), but there was evidence for a relaxation of selective constraint on direct-developing species (RELAX, $k = 0.30$, LRT = 12.08, $P = 0.001$). For the aquatic + fossorial partition, we did not find evidence of relaxed selection and instead found evidence of selection intensification with RELAX ($k = 2.51$, LRT = 12.08, $P = 0.001$) but did not find evidence to support positive selection with BUSTED (LRT = 0, $P = 0.5$). Finally, because we found that SWS2 was lost in a diurnal frog lineage (Dendrobatidae), we tested for relaxed selection on the remaining diurnal frog SWS2 but did not find evidence to support this ($k = 0.8$, LRT = 1.98, $P = 0.159$).

High Level of Variation in Frog Visual Opsins at Known Spectral-Tuning Sites

Each of the four visual opsins showed variation across frogs at gene-specific sites known to affect the spectral-absorbance profile of vertebrate visual pigments (known as spectral-tuning sites; Table 1). Some of this variation was previously identified in a smaller sample of frogs (Schott et al. 2022b), but our increased sampling has revealed variation at several additional spectral-tuning sites and a large number of new variants at previously noted sites (Table 1). In each of the opsins, there was overlap between known spectral-tuning sites and those inferred as being under positive or divergent selection (Table 1; supplementary table S1, Supplementary Material online, supplementary file S2, Supplementary Material online). A detailed analysis of potential spectral-tuning variation across frogs is presented in the supplementary results and discussion (Supplementary Material online).

Diurnally Active Frogs Maintain Dim-light Adaptive Residues in RH1 and SWS2

A previous study found that RH1 site 83 was conserved as N in frogs (Schott et al. 2022b) and this result was upheld with our larger dataset. This site and residue (N83) has been suggested to be associated with dim-light adaptation (Sugawara et al. 2010), but all frogs in our dataset had N83, including the 28 species with diurnal activity. Variation between A and S at RH1 site 299 affects retinal release rate in mammals (Dungan and Chang 2017). Frogs also exhibit variation between these two residues, and the two centrolenid (glass frog) species had V at this site, the effect of which is unknown, but may be similar to A due to the similarities between the two residues. Other RH1 sites known to affect kinetic rates, such as 59, 288, and 292 (Castiglione et al. 2017; Dungan and Chang 2017), were conserved across our sample of frogs. In frogs, SWS2 with T47 results in RH1-like dark-state stability, which is needed to achieve high light sensitivity necessary for dim-light visual function (i.e. low thermal isomerization rate; Kojima et al. 2017). All frogs in our dataset, including the diurnal species, had T47, though we note that dendrobatids, which are diurnal, appear to have lost the *SWS2* gene.

Frog Retinal Photoreceptors and Spectral Tuning of Frog Visual Pigments

To evaluate variation among frogs in photoreceptor complements and spectral sensitivities, and to provide additional context to our molecular results, we used MSP to measure photoreceptor spectral absorbances from 12 species including 10 adults and three tadpoles (13 specimens total). Maximum absorbances (λ_{max}) were estimated by curve fitting with the best-fitting of the A_1 or A_2 (Govardovskii et al. 2000) visual pigment templates (see Methods). In most species, the A_1 templates were the best fit for all cell types, but in several instances a second, smaller subpopulation of cells from a particular photoreceptor class had a better fit with an A_2 template (supplementary file S6, Supplementary Material online; Schott et al. 2024a). In all cases, the A_2 best-fit pigments had a blue-shifted peak absorbance relative to the A_1 best-fit pigments, which is opposite to the direction expected for A_2 visual pigments (Bridges 1972). Thus, the A_2 best-fitting cells are likely artifactual and were excluded from further analysis, except in *Spea multiplicata* where we found only best fit by A_2 templates for two photoreceptors. We include these here but note that the λ_{max} estimates for the two *S. multiplicata* photoreceptor classes may be biased as a result. Photoreceptor classes detected in each species and their corresponding absorbances are summarized in Fig. 5 and supplementary table S2, Supplementary Material online with complete results described in the supplementary results and discussion and supplementary file S6, Supplementary Material online (Supplementary Material online) and raw data available on Schott et al. (2024a).

Frogs Have a Wide Range of Spectral Sensitivities Across All Four Visual Pigments

We found green-sensitive RH1 rods in all species, with λ_{max} values ranging from 496 to 513 nm (Fig. 5; supplementary

Table 1 Variation in frog visual opsin sequences at known vertebrate spectral-tuning sites (based primarily on those identified in Hunt et al. 2001 and Yokoyama 2008 but see also supplementary results and discussion, Supplementary Material online)

Site (RH1 numbering)	Known from	Known spectral variants	Frog opsin variants			
			RH1	LWS	SWS1	SWS2
44	SWS2	M/T	M	M	M	M
46	SWS1/2	F/T/L	L/M	F	V/M/A/F/S/T/G/L/I	F
49	RH2, SWS1/2	S/F/A/V/L	L	A/I/G/L/F/S/C/V/T	L/I/F/V	I
52	RH2, SWS1/2	L/M/T/F	F/L	V/C/I/T	T/A/M	F/L
83	RH1/2	D/N	N	D	G	N
86	RH2, SWS1	M/T/F/S/L/Y	M	E	M/I	V
87	RH1, SWS1	V/D/C/A	V/I	T	C/S	I/V/L
90	RH1, SWS1	G/S/C	G	A	S/A/C	G/C
91	SWS1/2	V/I/S/P	F	S	I	S
93	SWS1/2	T/P/L/I	I/V	I	T/I/V/P/L/S	T/V/M
94	RH1/SWS2	A/S/C	T	S	V/G	A
96	RH1	Y/V	Y	F/I/A/V/C/S	V/I/M/L	Y
97	RH2, SWS2	T/A/S/C	T/S	N	S/N/A/C/T	S/T
102	RH1	Y/F	Y/F	Y	Y/C	Y
109	SWS1/2	V/A/G	G/T/A	L/M	V/A/F/T/I/M	A
113	RH1, SWS1	E/D	E	E	E/D	E
114	SWS1	A/G	G	G	G/A	G
116	SWS1/2	L/V/T	F/C/M/S	T	V/I/T/M	T/A/C
118	RH1, SWS1/2	S/T/A/G	T	S/A	T/S/A	T
119	RH1	L/F	L/F/T/I	V/T	L/V/P/F/T/	L
122	RH1, SWS2	E/I/Q/M	E	I	L/M	M/I
124	RH1	A/S/G/V	A/S/G	G/A	T/I/N	S/G
132	RH1	A/S/V	A/S	A	A	A
164	RH1, RH2, LWS	S/A	A	A/S	G/A	G/S/A
181	LWS	H/Y	E	H	E	E
194	RH1	P/R	L/P	G	V/I	V/I/A
195	RH1	N/A	K/S	S/N	G	N
207	RH1, RH2/SWS2	M/L	M	L	I/V/L	M/I/L
208	RH1	F/Y	F	M	F	F
211	RH1	H/C	H	C	C	C
261	RH1, SWS2, LWS	F/Y	F/Y	Y/F	F/Y	F
265	RH1, SWS1/2	W/Y	W/Y	W	Y/F	W
269	SWS2, LWS	A/S/T	A	T/A	A	A/E
292	RH1/2, LWS, SWS2	A/S	A	A/S	A	S
295	RH1	A/S	A	A	S	S
299	RH1	A/S	A/S/V	T	C	T
300	RH1	I/T/L	I/C	I	V	V
317	RH1	A/I/M/T	M/F	I/T	I	M/I

The residues we identified in frogs are listed for each spectral-tuning site (Frog Opsin Variants), with variation at that site known from a specific opsin in bold text. Underlined residues are newly reported variants not found previously in frogs (Schott et al. 2022b). Site numbers are based on bovine RH1 numbering.

table S2, Supplementary Material online). We also found evidence of a class of cones in this range in four species (λ_{max} 500 to 535 nm). These cones likely contain RH1 pigment but were variably red shifted relative to the RH1 rods in the same species by 5 to 22 nm. We also found evidence for blue-sensitive SWS2 rods in all species (λ_{max} 428 to 446 nm), with the exception of the dendrobatids where SWS2 rods have likely been lost. Absorbance spectra from frog cones are inherently noisy due to their smaller size and higher fragility, and, combined with their scarcity, this results in less precise cone measurements compared to rods. Long wavelength-sensitive (LWS) cones (552 to 589 nm) were recovered for all but three species. However, genetic data suggest that they are expected to be present in these species as well, so they may have been missed due to random sampling. The short wavelength-sensitive cones were only found in two species (*Callimedusa tomopterna*

and *D. auratus*, λ_{max} 411 and 441 nm, respectively) despite consistent *SWS1* expression across species. A detailed analysis of the molecular variation potentially underlying the spectral variation is presented in the supplementary results and discussion (Supplementary Material online).

Potential A₂ Chromophore Usage or A₁–A₂ Mixtures in Adult, Nonaquatic Frogs

Some of our MSP-derived spectral-absorbance curves have A₂ best fits, and λ_{max} values of the middle wavelength-sensitive cones suggest the potential for chromophore mixtures of A₁ and A₂. Thus, we used our eye transcriptome data to further investigate the potential that A₂ chromophore is present in the eyes of some adult, nonaquatic frogs. We did this by looking for expression of the *CYP27C1* gene, which encodes the cytochrome protein responsible for converting A₁ into A₂ chromophore (Enright
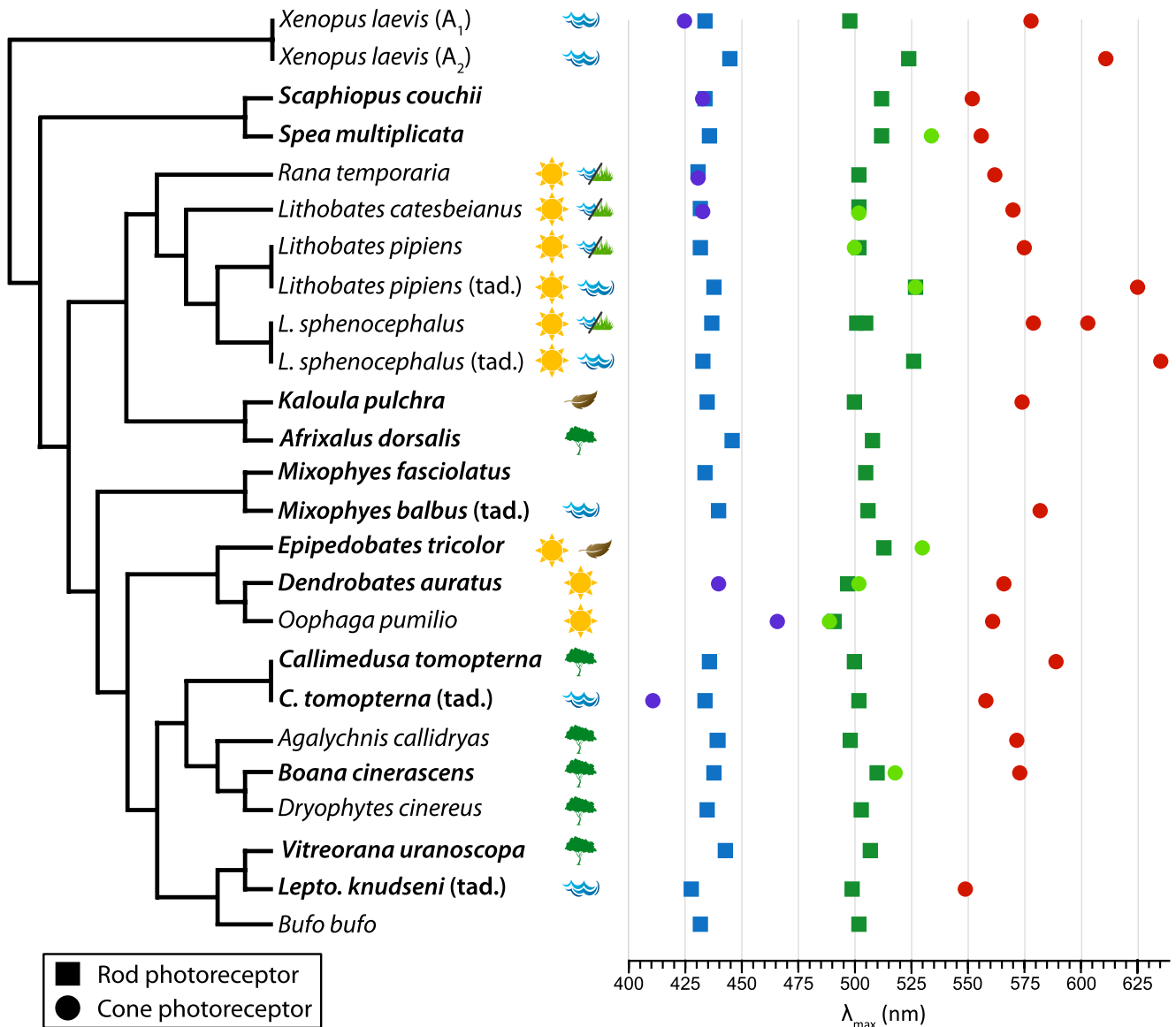
Fig. 5. Maximum absorbances (λ_{max}) of frog rod and cone photoreceptors. Data derived from the current MSP study (bold) and from previously published data as outlined below. Data from tadpoles are denoted with "tad." Colors correspond to visual pigment class. Phylogenetic relationships and traits follow those in Fig. 2. *Xenopus laevis* A$_1$ values were derived from *in vitro* expression and regeneration with A$_1$ (Starace and Knox 1998; Darden et al. 2003) or replacement of native A$_2$ with A$_1$ followed by MSP (Witkovsky et al. 1981). Data sources: *Xenopus laevis* (A$_2$) (Witkovsky et al. 1981), *Rana temporaria* (Koskelainen et al. 1994; Govardovskii et al. 2000), *Lithobates catesbeianus* (Hárosi 1982; Govardovskii et al. 2000), *L. pipiens* (Liebman and Entine 1968; Govardovskii et al. 2000), *L. sphenocephalus* (Schott et al. 2022a), *Oophaga pumilio* (Siddiqi et al. 2004), *Agalychnis callidryas* (Robertson et al. 2022), *Dryophytes cinereus* (King et al. 1993), and *Bufo bufo* (Govardovskii et al. 2000). Data from the current study, including sample sizes, are available in supplementary table S2, Supplementary Material online and supplementary file S6, Supplementary Material online (Supplementary Material Online) with raw data files on Schott et al. (2024a).

et al. 2015) in the same species for which we also have spectral-absorbance data. We were able to find at least a partial transcript in all species, indicating some level of expression of *CYP27C1*, with most species having complete or nearly complete transcripts (supplementary table S3, Supplementary Material online, Supplementary Material online; Schott et al. 2024a).

Discussion

We produced a phylogenetically and ecologically broad dataset of frog visual opsin genes to comprehensively

assess the complement, variation, and evolution of frog visual systems at the molecular level and to test several hypotheses of visual opsin functional adaptation. This approach revealed considerably more variation in visual opsin sequences than was previously evident (Schott et al. 2022b), including additional variation at spectral-tuning sites known from other vertebrates, and at many novel sites that may be involved in spectral and/or nonspectral function and adaptation. Our results support the loss of *SWS2* in dendrobatid frogs and provide preliminary evidence for the loss of *SWS1* in arthroleptids. We found no evidence for gene duplication beyond the *RH1* and *LWS*

duplications identified previously in *Xenopus laevis* and *Pyxicephalus adspersus*, respectively (Feehan et al. 2017; Schott et al. 2022b). We identified significant evidence for positive selection on three of the four frog visual opsin genes and shifts in selective pressure associated with habitat usage and life history, but not activity pattern. These findings strongly support functional adaptation in visual opsins across the frog radiation. Consistent with this, we found a wide range of spectral sensitivities in frog visual pigments using microspectrophotometry (MSP), including potential variation in the usage of A_1 and A_2 chromophore mixtures.

Visual Opsin Gene Duplications and Loss in Frogs and Other Vertebrates

Ancestrally, vertebrates had five visual opsin genes (*RH1*, *RH2*, *LWS*, *SWS1*, and *SWS2*), but different lineages have decreased or increased this initial set of opsins through gene loss and duplication (Lamb et al. 2016). Amphibians lost the *RH2* cone opsin early in their evolutionary history (Donner and Yovanovich 2020; Schott et al. 2022b) and this level of gene loss is lower than that inferred for other ancestrally nocturnal groups including mammals (*RH2* and *SWS1* [monotremes] or *SWS2* [therians]), snakes (*RH2*, *SWS2*), geckos (*RH1*, *SWS2*), and crocodilians (*RH2*, *SWS1*) (Gemmell et al. 2020). The relatively limited gene loss in frogs may be explained by many species being highly visual predators, including nocturnal species, as reflected in their large eye size and investment relative to other vertebrates (Thomas et al. 2020). The loss of *RH2* is a common theme in ancestrally nocturnal lineages (with the exception of geckos, which instead lost the rod opsin, *RH1*). RH2 loss might have been favored by the overlapping spectral sensitivities between RH1 and RH2 (both typically around 500 nm; Davies et al. 2012), which likely leads to a redundancy of RH2 in species primarily active in low light, where RH1 is more useful. In other vertebrate groups, adaptation to more extreme dim-light environments led to loss of additional visual opsin genes including in deep-diving whales (Meredith et al. 2013) and deep-sea teleost fishes (Lupše et al. 2021), as well as in fossorial caecilian amphibians (Mohun et al. 2010), snakes (Gower et al. 2021), and mammals (Emerling and Springer 2014). We found no evidence of a similar pattern in frogs, but the current data from species inhabiting such extreme dim-light environments are limited. For instance, species of *Pipa* have some of the smallest relative eye sizes among frogs and inhabit extremely murky water (Thomas et al. 2020), but the two *Pipa* species in our dataset had copies of each visual opsin, although the *SWS2* sequence recovered from *P. carvalhoi* was partial. Additionally, of the three fossorial species we sampled, *Rhinophrynus dorsalis* expressed all four frog visual opsins, *Glyphoglossus guttulatus* did not express *SWS2*, and the transcriptome of *Myobatrachus gouldii* was low quality, with many genes not recovered due to a low read count. Thus, the loss of *SWS2* in *G. guttulatus* is an interesting possibility that requires further investigation. Remarkably, the

two better supported instances of gene loss in frogs are not associated with shifts to lower-light levels, and some actually occur in diurnally active species.

There is strong evidence for the loss of *SWS2* in dendrobatids, and corresponding loss of the blue-sensitive rods where SWS2 is typically expressed in frogs. We did not find *SWS2* expressed in the dendrobatid eye transcriptomes, and another study was also unable to recover SWS2 from dendrobatid bait-capture data or an eye transcriptome (Wan et al. 2023); however, in the two dendrobatid genomes, we found short fragments that are likely pseudogene remnants of *SWS2*, based on phylogenetic analysis. Furthermore, retinal microspectrophotometry (MSP) to estimate photoreceptor absorbance spectra did not detect blue-sensitive rods in the three dendrobatids examined here or the species examined previously (Siddiqi et al. 2004). Dendrobatids are primarily ground-dwelling, diurnal frogs, and thus the loss of *SWS2* and blue-sensitive rods may be explained by a reduced benefit of the increased breadth of dim-light spectral sensitivity that these photoreceptors provide. Although we found evidence for a relaxation of selective constraint on diurnal frog *SWS2* based on the HYPHY RELAX model, this was a relaxation in the strength of positive selection. We did not find any evidence for a difference in selection pressures with PAML CmC, and all species in our dataset (including the diurnal ones) maintain the SWS2 mutation (T47) that increases dark-state stability and thus light sensitivity (Kojima et al. 2017). Together, these results suggest a generally conserved function of SWS2 across nocturnal and diurnal frogs. Interestingly, some salamander lineages have also lost blue-sensitive rods (thought to be ancestrally plesiomorphic in frogs and salamanders) but not *SWS2* (Takahashi et al. 2001). In salamanders, SWS2 is expressed in both blue-sensitive rods and in cones, and no studied species have the T47 mutation that results in rod-like pigment stability. This raises the question of whether blue-sensitive rods function differently in salamanders versus frogs and if this cell type is truly homologous between both groups.

The two arthroleptids in our dataset, one with diurnal activity (*Arthroleptis poecilonotus*) and one nocturnal (*Leptopelis aubryi*), lacked *SWS1* gene expression. Unfortunately, there is no genomic data for arthroleptids, which is needed to confirm gene loss, and SWS1 cones are difficult to detect with MSP (detailed below). However, the apparent shared lack of expression in this family warrants further investigation. For example, *SWS1* expression may be restricted to the tadpole stage in this family, which includes both biphasic and direct-developing species. This would differ from the pattern seen in leopard frogs (*Lithobates sphenocephalus*), where all visual opsins were found to be expressed at both life stages (Schott et al. 2022a), but differential usage of opsins across life stages is common in teleost fishes (Carleton et al. 2020). Further studies (e.g. genomic, transcriptomic, immunolabeling) that incorporate additional species and life stages of arthroleptids will be needed to resolve the question of whether the *SWS1* gene was lost in this family.

Opsin gene duplication in tetrapods is rare and most known instances have occurred in nontetrapods (specifically teleost fishes; Musilova et al. 2021). In tetrapods, known duplications are restricted to mammals (some marsupials and primates; Cowing et al. 2008; Carvalho et al. 2017), snakes (Hauzman et al. 2021; Rossetto et al. 2023), and frogs (Feehan et al. 2017; Schott et al. 2022b). Several frog species are polyploids, and thus may have more than one functional copy of each opsin gene, although often one of the homologs is lost. The African clawed frog (*Xenopus laevis*), for instance, is an allotetraploid (Session et al. 2016) and has two *RH1* homologs (one of which was further duplicated; Feehan et al. 2017), but for each of the other visual opsin genes, we found evidence that one of the two copies was pseudogenized. We did not find any additional strong evidence for visual opsin gene duplication in frogs, but it can be difficult to distinguish gene duplications from other types of variation based on transcriptomic data alone. In several species, we found more than one transcript reconstructed for a single gene, but these all appear to be polymorphisms or transcript variants (either real or due to incomplete and/or incorrect de novo assembly or gene predictions). A combination of genomic and transcriptomic sequencing will be required to evaluate whether opsin transcript variants are present in frogs and what functional consequences they may have.

Signatures of Selection in Visual Opsins Associated With Differences in Ecology

Previous work using a smaller dataset (33 species) found evidence for positive selection on two of the four frog visual opsin genes (*RH1* and *LWS*), as well as substantial variation at spectral-tuning sites and sites that may affect other aspects of visual pigment function, such as the speed of light activation and the stability of the dark state (Schott et al. 2022b). With our enhanced dataset of 122 species, we additionally found evidence for positive selection on *SWS2*, albeit at a smaller proportion of sites than for either *RH1* or *LWS*. We did not find evidence for positive selection on *SWS1*, despite this gene being under the lowest overall selective constraint among the visual opsins. This pattern is opposite to that found in a sample of 68 to 107 reptiles (including birds), where *SWS1* was the visual opsin under the highest constraint (Gemmell et al. 2020). We also found frog *SWS1* to have significant variation in selective constraint among lineages, as well as the highest amount of variation at previously identified spectral-tuning sites. Unfortunately, the functional importance of the SWS1 visual pigment in frogs is also the least well understood. Evidence for SWS1 photoreceptors is sparse, presumably due to their small size and rarity in the retina. For instance, *SWS1* was estimated to have the lowest expression among the visual opsins in a differential expression study of vision genes in leopard frogs (*Lithobates sphenocephalus*; Schott et al. 2022a) and this photoreceptor class was found to be small and rare in

the retinas of bullfrogs (*L. catesbeianus*; Hisatomi et al. 1998) and African clawed frogs (*X. laevis*; Starace and Knox 1998). Yet, the consistent expression of *SWS1* in the eye across frogs (except arthroleptids, as noted above) and strong selective constraint (albeit weaker than the other visual opsins) suggests that SWS1 contributes an important and functionally conserved part of the frog visual repertoire.

In addition to phylogeny-wide tests of positive selection for each visual opsin, we tested for differences in selective constraint associated with differences in activity pattern, habitat, distribution (seasonality), and life history among species. We did not find that activity pattern or distribution were primary drivers of selective shifts on visual opsins but did find significant effects associated with differences in habitat and life history. This is consistent with similar patterns in teleost fishes where the spectra of available light and life history appear to have driven visual system adaptation (Carleton et al. 2020) but differs from patterns in squamates and birds where shifts in activity pattern are strongly associated with positive and divergent selection on visual opsins (and other visual genes; Simões et al. 2016; Wu et al. 2016; Hauzman et al. 2017; Schott et al. 2018). The pattern we found in frog visual opsins differs, in part, from that in nonvisual opsins, where activity pattern and distribution are associated with differences in selection. These associations may be explained by the role of some nonvisual opsins in circadian rhythms and seasonal responses, although selective shifts of nonvisual opsins among species with differences in habitat and life history were also found (Boyette et al. 2022).

Aquatic and fossorial frogs have smaller eye size and lower investment than species with other lifestyles, including semiaquatic and subfossorial (Thomas et al. 2020). This is attributed to the lower-light availability in the subterranean environments inhabited by fossorial species, and in the murky ponds and pools within which aquatic frogs hunt and breed, leading to less reliance on vision (Duellman and Trueb 1994; Thomas et al. 2020). Accordingly, we predicted that there would be a relaxation of selective constraint on the visual opsin genes of aquatic and fossorial species. For the two rod-expressed pigment genes (*RH1* and *SWS2*), we did not find evidence of relaxed selection on aquatic and fossorial frogs relative to other species. We did find, however, significant differences in selective pressure in the cone-expressed *LWS* and *SWS1* and found elevated ω in aquatic and fossorial species (based on CmC) in both genes. For both genes, we found evidence that the higher ω stems from a relaxation of selective constraint (based on RELAX analyses). These findings align with our predictions that visual opsins in fossorial and aquatic species are under relaxed selective constraint, which we hypothesized is due to lower eye investment. However, in *SWS1*, we also found evidence for relaxed selection in semiaquatic frogs, which does not align with our expectations because semiaquatic frogs do not have lower eye investment (Thomas et al. 2020). Somewhat contradictory to the RELAX results, the BUSTED method supported

positive selection in aquatic and aquatic + fossorial (but not in semiaquatic) species with the best-fitting partition being aquatic. This result points to potential adaptive evolution in *SWS1* to the environment in aquatic species but must be interpreted cautiously due to the lack of corroborating evidence from the other methods (CmC or RELAX). By contrast, in *LWS*, we found evidence for positive selection in aquatic and fossorial species (using BUSTED), despite a lack of evidence for positive selection in aquatic species alone. The positive selection in aquatic and fossorial species was weaker than in other frogs ($\omega = 3.4$ vs. 10.7), but at a higher proportion of sites (3.1% vs. 0.46%). This pattern suggests that, in addition to an overall relaxation of selective constraint, *LWS* may have undergone adaptation to the generally lower-light environments inhabited by aquatic and fossorial species. To our knowledge, no studies have yet examined nonspectral functional changes in LWS visual pigments to confirm this possibility. Our findings highlight the need for such functional studies in frogs and other vertebrates.

In contrast to aquatic and fossorial species, scansorial (including arboreal) frog species have larger eyes and higher eye investment. Larger eyes are hypothesized to provide higher visual acuity, which would be particularly beneficial in navigating complex, three-dimensional arboreal environments (Thomas et al. 2020). In addition, the lenses of scansorial frogs transmit significantly less short-wavelength light than those of other species, which is also likely to increase visual acuity (Thomas et al. 2022a). Based on this, we hypothesized that scansorial species may have undergone adaptive evolution of their visual opsins and hence show shifts in selective pressure and positive selection. Indeed, we found evidence of differential selective pressure in scansorial frogs on two of the visual opsins, *RH1* and *SWS1* (based on CmC); however, these genes showed opposite patterns of selection, with higher ω in scansorial species for *RH1* and lower ω for *SWS1*. Thus, these results provide only partial support for our hypothesis. For *RH1*, there was no evidence for relaxed selection, which is consistent with our predictions, but the estimated ω for the positively selected site class was only slightly higher in scansorial species using both RELAX and BUSTED and both at a small proportion of sites. This result likely explains the elevated ω that was detected by CmC. Although these results suggest that *RH1* is evolving differently in scansorial versus nonscansorial frogs, the functional ramifications of this pattern are unclear. One possibility is selection for increased temporal resolution in scansorial frogs through faster RH1 kinetics, which would benefit species that navigate and hunt in complex arboreal habitats under dim-light conditions. Temporal resolution of scotopic vision is limited, at least in part, by the speed of rod recovery (Fortenbach et al. 2015). Most research in this area has focused on responses to bright flashes, finding that the rate-limiting step in recovery time is the downstream shutoff of signaling by the phototransduction protein RGS9 (Peinado Allina et al. 2017). Responses to dim flashes, which are more likely to

represent a natural scenario encountered by nocturnal scansorial frogs, are less well understood (Peinado Allina et al. 2017). Coevolutionary changes to the phototransduction cascade and visual processing speeds would likely also be needed to improve temporal resolution. The contribution of RH1 to these changes could be tested through in vitro expression and functional kinetic assays.

For the final visual opsin gene, *SWS2*, we found that direct-developing species have significantly higher ω than other species. RELAX analyses suggest this elevated ω is due to a relaxation of both negative and positive selection. This opsin is differentially expressed between leopard frog tadpoles and juveniles, suggesting a difference in the importance, and perhaps function, of blue-sensitive rods among life stages (Schott et al. 2022a), similar to the differences in opsin expression palettes between larvae and adults of many teleost fishes (for a review see Carleton et al. 2020). This relaxation of selection may in turn reflect relaxed functional constraints on blue-sensitive rods and SWS2 in direct-developing species which, by lacking a tadpole stage, are not constrained to a dual functional role in this photoreceptor. Functional studies examining blue-sensitive rods in tadpoles are required to evaluate this possibility.

Kinetics of RH1 With Respect to Dim Light and Freshwater Adaptation in Frogs Versus Fishes

Many frogs inhabit turbid, red-shifted freshwater as tadpoles, and some continue to use these environments as adults, whereas other species metamorphose to life on land, and direct-developing species lack the aquatic tadpole stage altogether. Despite this diversity in reliance on freshwater habitats, we found no evidence that the RH1 residues identified as functionally significant in freshwater fishes are associated with freshwater use in frogs. In particular, a study in croakers (teleost fishes) demonstrated that the shift from a marine to freshwater habitat was accompanied by positive selection and a suite of substitutions at four RH1 residues (119, 122, 124, and 261) that result in red-shifted RH1 pigment absorbance and faster kinetics, and are hypothesized to increase the speed of dark adaptation (Van Nynatten et al. 2021). Besides croakers, these substitutions are found in several other freshwater fish lineages and are suggested to form a general basis for adaptation to turbid, red-shifted freshwater environments (Van Nynatten et al. 2021). For three of those sites (119, 122, and 261), we found that most frogs have the same residues as the marine croaker ancestor (and bovine RH1), and not those of freshwater fish lineages. Frogs share residues with freshwater fishes at the fourth site, 124, at which an A to S substitution causes increased kinetic rates (lower-light-activated stability) and a slight blue shift in fishes (Castiglione and Chang 2018; Van Nynatten et al. 2021), but there is no consistent pattern in the ecology or life history of frog species with S124. The lack of a shared basis for adaptation to freshwater environments in frogs and fishes is perhaps expected because E122 was

previously found to be conserved in tetrapods due to a functional constraint to maintain rod photosensitivity (Castiglione and Chang 2018). This is a result of a trade-off between increased kinetic rates, which can augment the speed of dark adaptation, and increased photosensitivity, which requires high stability and thus lower kinetic rates (Castiglione and Chang 2018). It has been proposed, that this trade-off may be offset by an increased benefit of faster dim-light adaptation when navigating turbid freshwater environments, which have sharp transitions between bright- and dim-light conditions caused by rapid light attenuation with depth (Van Nynatten et al. 2021). Aquatic frogs, which need to periodically surface to breathe, and semiaquatic frogs, which occasionally dive below the surface, might also benefit from faster rates of dark adaptation. If faster rates are indeed beneficial for (and present in) aquatic and semiaquatic species, our results indicate that they were achieved through a set of substitutions different from those in freshwater fishes.

Another site responsible for differences in RH1 kinetic rates is site 83 (Sugawara et al. 2010; Bickelmann et al. 2012). Previous work found that frogs are conserved for N at this site (Schott et al. 2022b), and this is also the case in our larger dataset. N83 has been proposed to be a dim-light adaptation due to decreased kinetic rates (higher light state stability) thereby increasing photosensitivity (Bickelmann et al. 2012), but N83 is not restricted to nocturnal or dim-light adapted vertebrates (Schott et al. 2022b) and is present in all frogs in this study, including those with diurnal activity. N83 is also present in both marine and freshwater croakers and thus does not appear to be related to freshwater adaptation in that group. In cichlids, N83D is associated with a transition to brighter, clear-water environments (Hauser et al. 2017), but a similar pattern is not seen in frogs that inhabit bright light environments. The slowest kinetic rate (highest light state stability), and therefore highest potential photosensitivity (Dungan and Chang 2017) was found with the combination N83, A292, and S299 when mutated in bovine RH1 (Dungan and Chang 2017). A292 is conserved across our frog sample, whereas 299 varies between A, S, and V. We found no correlation between S299 and utilization of low light environments suggesting that frog RH1 has slower kinetic rates consistent with dim-light adaptation through higher photosensitivity, and that functional adaptation of these rates, if present, occurred through pathways distinct from those currently known in other lineages.

Molecular Basis of Visual Pigment Sensitivity and Variation in Frog Photoreceptors

Using our large sample of frog visual opsins, we identified substantial amounts of sequence variation at previously identified spectral-tuning sites including 38 new frog variants at opsin-specific sites (61 including nonopsin-specific tuning site variants). This tuning site variation suggests considerable diversity in frog visual pigment spectral absorbances, which in turn may be associated with differences in habitat, activity pattern, and life history. To begin to explore these potential differences and place our molecular results in context, we assessed photoreceptor spectral absorbances from 12 species using MSP and combined this with previous results from another nine species.

We found broad support for the prediction that the molecular variation in frog visual opsins is associated with considerable variation in visual pigment spectral absorbance. The new data from our MSP analyses has extended the range of spectral absorbance (λ_{max}) in one or both directions for each of the four frog visual pigments. We discuss in detail the potential molecular basis for the spectral differences in the supplementary results and discussion (Supplementary Material online) but note here that differences at known spectral-tuning sites only account for a proportion of the observed variation. Some key frog spectral-tuning site variation previously known from other vertebrates appears to include: (1) F261Y in RH1, which is known to cause a 10 nm shift in bovine RH1 (Chan et al. 1992); (2) I116T in SWS2, which results in a −7 nm shift in bluefin killifish SWS2 (Yokoyama et al. 2007); and (3) A164S/S164A in LWS, which shift λ_{max} by 6 and −7 nm, respectively, in mammalian LWS (Asenjo et al. 1994; Yokoyama et al. 2005, 2008). Our data implicate several other sites as being involved in frog spectral tuning (e.g. 144, 169 [RH1]; 164, 217 [SWS2]; 100, 108, 111, 115 [SWS1]) providing a starting point for future functional studies that will broaden our understanding of the basic mechanisms of vertebrate visual opsin spectral tuning, with potential practical applications for bioengineering and optogenetics.

The high level of variation in frog SWS1 suggests that some species may have SWS1 pigments maximally sensitive to UV wavelengths (Schott et al. 2022b), although to date only pigments maximally sensitive to the violet range have been identified. Salamanders have the opposite pattern with SWS1 pigments maximally sensitive to UV wavelengths, with no known shifts to violet sensitivity (with the possible exception of *Notophtalamus viridescens*; Korenyak and Govardovskii 2013; Mège et al. 2016). This difference in the sensitivities of frog (specifically *X. laevis*) and salamander SWS1 pigments was linked to mutations at seven residues (86, 91, 93, 109, 113, 116, and 118), with F86M and T93P together being responsible for a 35 nm shift from UV sensitivity (359 nm) to violet sensitivity (394 nm) in an inferred ancestral pigment (Takahashi and Yokoyama 2005). Neither mutation alone causes a spectral sensitivity shift, and most frogs do not have the residues present in *X. laevis*: T93 is the most common, but no species has F86. Goldfish (*Carassius auratus*) also have UV-sensitive SWS1, yet the single mutations F86M and Q93T do not change the λ_{max} from UV (~358 nm), although the double mutant has not been tested (Yokoyama and Shi 2000; Cowing et al. 2002). This suggests that further sampling of frog SWS1 spectral sensitivities will reveal additional variation (perhaps into the UV range) and increase our general understanding of SWS1 spectral tuning.

In addition to the expected long (LWS) and short (SWS1) wavelength-sensitive cones, we found a third cone type in four species that is maximally sensitive to middle wavelengths (λ_{max} of 500 to 535 nm). These cones are similar to the green-sensitive RH1 rods, but red shifted by 5 to 22 nm. Similar cones have previously been found in two *Lithobates* species and *Oophaga pumilio* (Liebman and Entine 1968; Hárosi 1982; Siddiqi et al. 2004), but these did not show similar red-shifting. In any other vertebrate group, it might be assumed that the opsin identity of these pigments was RH2, but there is strong evidence that this gene was lost early in amphibian evolution (Schott et al. 2022b), and we found no evidence for a gene duplication that could explain this pattern. Thus, the most likely visual opsin identity of these pigments is RH1, but this requires an explanation for the red shifted λ_{max}. This would make frogs a rare example of RH1 expression in a cone and potentially the only example of an RH1 pigment expressed in a "true" cone. In other known examples of RH1 cone expression (e.g. in lizards and snakes), RH1 is expressed in cone-like cells evolutionarily derived from rods, and these species lack RH1 rods (McDevitt et al. 1993; Schott et al. 2016). It remains possible that, instead, frog RH1 cones are developmentally derived from a subpopulation of RH1 rods rather than from a cone population that co-opted RH1 expression. This distinction could have implications for whether RH1 interacts with a rod or cone transducin (and other downstream rod or cone phototransduction proteins) and for the functional role of this photoreceptor cell type.

Some of the variation observed in our MSP data, especially variation for which we did not find a molecular spectral-tuning basis, suggests that at least some frog species use visual pigments with mixtures of A_1 and A_2 chromophores. Indeed, in most of our transcriptomes, we found expression of the *CYP27C1* gene, which encodes the cytochrome protein that converts A_1 to A_2 (Enright et al. 2015), consistent with a scenario of chromophore mixtures contributing to variation in spectral absorbance. The most compelling instances are the middle wavelength-sensitive cones, but only one of the species had absorbance spectra best fit by an A_2 template, and the measurements were based on small sample sizes. This explanation would also require variation in the incorporation of A_2 among different photoreceptor types. An alternative (but not mutually exclusive) explanation is the coexpression of more than one visual opsin in the same photoreceptor type, which is an alternative mechanism for spectral tuning in some vertebrates (Isayama and Makino 2012; Carleton et al. 2020). Visual opsin coexpression has been found in salamander cones (Isayama and Makino 2012; Isayama et al. 2014), but secondary pigments are expressed at much lower levels and therefore do not substantially affect absorption properties. Further work will be needed to directly quantify the A_1 versus A_2 chromophore contents of frog retinas (e.g. using high performance liquid chromatography; Enright et al. 2015) and to localize expression of mRNA and proteins to specific photoreceptor cell populations.

Conclusions

Frogs are a remarkable system for studies of visual evolution and adaptation due to their diverse ecologies, life histories, and behaviors combined with their highly visual nature. Nevertheless, frog vision remains understudied relative to that of other major vertebrate lineages. Recent studies have begun to provide evidence for visual adaptation in eye morphology and ocular media across the frog tree of life, but investigations of molecular aspects of visual adaptation are limited. Here, we created a large, taxonomically, and ecologically diverse dataset of frog visual opsins to elucidate how these animals have adapted to distinct visual environments at the molecular level. Relative to other ancestrally nocturnal vertebrate lineages, frogs appear to have lost the fewest visual opsin genes, reflecting their strong reliance on the visual sense. In vertebrates, the use of more light-limited environments is correlated with visual opsin loss, but we highlight that this trend appears absent in frogs. Instead, we found strong evidence for the loss of *SWS2* in a diurnal lineage of frogs (dendrobatids) and preliminary evidence for the loss of *SWS1* in a lineage containing both diurnal and nocturnal species (arthroleptids). The visual opsin sequences of frogs are highly variable, including at known spectral-tuning sites, and we found evidence of positive selection and shifts in selective pressure associated with habitat usage and life history. Combined, these results suggest extensive functional adaptation across the frog tree of life, a scenario corroborated by the wide range of spectral sensitivities we found in the visual pigments of a subset of species. Our findings indicate that visual opsin variation at known spectral-tuning sites can account for only some of the observed variation, suggesting that frog spectral tuning has occurred through pathways not known in other vertebrates. Other spectral-tuning mechanisms are likely also involved, including variation in the use of A_1 and A_2 chromophore mixtures and opsin coexpression. Revealing the spectral-tuning mechanisms of frog opsins will provide a better understanding of how these animals have adapted to their diverse light environments. This effort will broaden our understanding of the fundamental mechanisms of spectral tuning across vertebrates, with potential applications for bioengineering and optogenetics.

Materials and Methods

Species Sampling

Frog samples were obtained from wild populations in Australia, Brazil, Cameroon, Ecuador, Equatorial Guinea, French Guiana, Gabon, Seychelles, United Kingdom, and the United States, as well as through captive breeding programs and the pet trade. A complete list of specimens is available in supplementary file S1, Supplementary Material online. Generally, individuals were kept in complete darkness (i.e. dark adapted) for three or more hours prior to euthanasia via immersion in a solution of MS-222 following approved animal care procedures (NHMUK, NMNH 2016-012, UNESP Rio Claro CEUA-23/2017, UTA A17.005,

ANU A2017/47). Several samples were not dark adapted prior to sampling, but this should not affect the recovery of the visual opsins (Schott et al. 2022a). Whole eyes were extracted and placed in RNAlater (Ambion) for at least 24 h at 4°C prior to storage at −80°C. Some samples were collected at remote field sites and were kept as cool as possible prior to freezing at −80°C. Voucher specimens and tissues for further genetic analysis were accessioned in natural history museums (supplementary file S1, Supplementary Material online).

Transcriptome Sequencing and Assembly

Total RNA was extracted from whole eyes using the Promega Total SV RNA Extraction kit (Promega). Tissue was homogenized in the prepared lysis buffer using the Qiagen Tissuelyser (10 min at 20 Hz). Messenger RNA library construction was performed using the Kapa HyperPrep mRNA Stranded with RiboErase kit (Roche). Each indexed sample was pooled in equimolar amounts and sequenced with paired end 150 bp reads on a HiSeq4000 at the QB3 Genomics Core at University of California, Berkeley or a NovaSeq6000 at the North Texas Genome Center (University of Texas at Arlington).

Prior to assembly, adapters, low quality bases, and short reads were removed with either Trimmomatic (Bolger et al. 2014) or TrimGalore! (https://www.bioinformatics.babraham.ac.uk/projects/trim_galore/), which implements Cutadapt (Martin 2011). Quality of processed reads was assessed with FastQC (http://www.bioinformatics.babraham.ac.uk/projects/fastqc/). Transcriptome assembly of each sample was performed de novo using Trinity (Grabherr et al. 2011) incorporating all paired reads following the standard protocol. To evaluate the expression of similar *LWS* homologs in the *Pyxicephalus adspersus* eye transcriptome, the trimmed reads were mapped to the coding sequences of the visual opsins extracted from the *P. adspersus* genome using BWA-MEM (Li 2013) and the consensus sequences extracted following a modified version of the assembly pipeline from Schott et al. (2017) (see Schott et al. 2024a).

Visual Opsin Sequence Dataset

Visual opsin coding sequences were extracted from the assembled frog eye transcriptomes using NCBI BLASTn and reference sequences previously obtained from frogs (Schott et al. 2022a, 2022b). We used the discontiguous megablast approach with an e-value cutoff of 1×10^{-10} to identify transcript hits, which were imported into MEGA, aligned with the reference, and manually trimmed to the coding sequence ensuring the longest open reading frame was recovered. Gene identifications were confirmed by BLAST searches against the NCBI nucleotide database and later by phylogenetic analysis. Partial transcripts of the same gene (e.g. due to incomplete transcript assembly or sequence coverage) were combined to produce as complete a coding sequence as possible. We took this somewhat more intensive approach because we have found

that fully automated approaches often produced incomplete or incorrect transcripts. We combined the eye transcriptome data with the dataset of Schott et al. (2022b), which included visual opsins obtained from retinal cDNA sequencing, and sequences extracted from publicly available data (transcriptomes, genomes, and Genbank), as well as an additional five published frog genomes and one prepublication draft genome assembly (*Atelopus zeteki*; Gratwicke B, Koepfli K-P, Mudd A, and Rokhsar D, unpublished). Our combined sampling includes 122 species, representing 34 of the 56 currently recognized frog families (Fig. 2; supplementary fig. S1, Supplementary Material online).

Phylogenetic and Selection Analyses

Coding regions for each of the four frog visual opsin genes (*RH1*, *LWS*, *SWS1*, and *SWS2*) were aligned using codon alignment (MUSCLE, as implemented in MEGA; Edgar 2004; Tamura et al. 2011) followed by manual editing to remove terminal stop codons and unique insertions and to trim nonhomologous regions that were due to annotation errors or transcript variants. Gene trees for each opsin ("gene tree") were inferred by Maximum Likelihood (ML) using PhyML 3 (Guindon et al. 2010) under the GTR + G + I model with a BioNJ starting tree, the best of NNI and SPR tree improvement, and aLRT SH-like branch support (Anisimova and Gascuel 2006). Because individual gene trees do not always reflect species' evolutionary histories, it is a common approach in selection analyses to compare results from gene-tree topologies to those that reflect the current understanding of species evolutionary relationships (species-tree topology) to ensure that results are robust to minor topological differences (Schott et al. 2018; Van Nynatten et al. 2021). To produce species-tree topologies for each gene, we generated a topology that matched expected species relationships based on several large-scale phylogenies (Pyron and Wiens 2011; Fig. 1; Feng et al. 2017; Jetz and Pyron 2018; Streicher et al. 2018) and trimmed these to match the taxon sampling of the individual genes. If multiple transcripts/sequences for the same species and gene were recovered, we kept the longest. Differentiated full length multiples were both included but if sequences were identical at the protein-level one was randomly removed.

To estimate the form and strength of selection acting on the visual opsin genes, we analyzed the sequence alignments and both the original and adapted gene trees using codon-based likelihood models implemented in the codeml program of the PAML 4 software package (Yang 2007). Specifically, we used the random sites models (M0, M1a, M2a, M2a$_{rel}$, M3, M7, M8a, and M8) to infer phylogeny-wide selection patterns and to test for positive selection acting on a subset of sites in each gene. Moreover, we used clade model C (CmC; Bielawski and Yang 2004) to test for long-term shifts in selection pressures associated with differences in activity pattern, adult habitat, seasonality, and life history (ecological partitions,

see below). CmC allows for tests of differences in selective regimes at a subset of sites between two or more partitions of a tree, which can identify long-term shifts in selection pressure associated with changes in ecology and function (Schott et al. 2014, 2019; Torres-Dowdall et al. 2015; Baker et al. 2016; Dungan et al. 2016; Castiglione et al. 2017; Hauser et al. 2017; Hauser et al. 2021; Van Nynatten et al. 2021; Castiglione et al 2023a, 2023b). To determine significance, model pairs were compared using a likelihood ratio test (LRT) with a χ^2 distribution to the null model, M2a$_{rel}$ (Weadick and Chang 2012). The likelihoods of each of the significant partitions were compared to determine the best-fitting partition overall for each gene. The Bayes Empirical Bayes (BEB) approach was used to identify individual sites with a posterior probability >80% of being in the positively selected class of sites. All PAML analyses were run using the BLASTPHYME interface (Schott et al 2019b) with varying starting ω values (1, 2, 3) to avoid potential local optima. If models failed to converge (worse likelihood score than null model) we increased the range and frequency of starting values (e.g. 0.5 intervals from 0.5 to 3.5). BLASTPHYME automatically selects the models with the best likelihoods among the replicates.

We also analyzed the data using the HYPHY models FUBAR (Pond and Frost 2005; Murrell et al. 2013), BUSTED (Murrell et al. 2015), and RELAX (Wertheim et al. 2015) implemented on the Datamonkey web server (Delport et al. 2010). FUBAR uses a hierarchical Bayesian method to average over a much larger number of site classes than the PAML models and allows for an independently estimated value for d_S. BUSTED provides an alternative approach for identifying episodic positive selection across a gene and can be used either on an entire phylogeny (similar to the PAML M2a test) or on separate foreground and background partitions (similar to the PAML branch-site and clade models). Notable differences include synonymous rate variation, no specified neutral site class, and no constraint that the proportion of sites in a site class be equal between the null and alternate models. We used this model to test for gene-wide positive selection and to test for positive selection specifically on the significant partitions identified by PAML CmC. Finally, RELAX is a model designed to test for the relaxation of selective constraint acting on a subset (e.g. a partition) of a phylogenetic tree based on the Branch-site REL model (Kosakovsky Pond et al. 2011). It uses three site classes partitioned between the foreground (test) and background (reference) branches under the constraint that $\omega_{foreground} = \omega_{background}^k$. The exponent k is the selection intensity parameter where a $k < 1$ indicates a relaxation of selection intensification (values of ω move toward 1, becoming smaller if >1 and larger if <1), whereas an $k > 1$ indicates an intensification of selection (values of ω move away from 1). We used RELAX to test for relaxation and intensification of selection on the significant partitions identified by CmC. This method has successfully been applied to test for relaxed selection on opsin genes in several lineages

including cichlids, bats, butterflies, and mirid bugs (Gutierrez et al. 2018a, 2018b; Hauser et al. 2021; Xu et al. 2021; Mulhair et al. 2023). The HYPHY models each automatically inferred gene trees with the GTR model, which were rerooted on *Ascaphus truei* prior to analyses.

Species Trait Classification

Frog species were partitioned into binary trait categories that we hypothesize may influence the evolution of visual detection of light: adult activity period, adult ecological habitat, distribution and seasonality, and life history. There is strong support that the most recent common ancestor of extant frogs was nocturnal (Anderson and Wiens 2017), as are the vast majority of extant frog species. Based on this, species were partitioned for adult activity period to contrast the presence of diurnal activity versus no diurnal activity. To test the effect of distinct light environments associated with adult ecological habitats, species were partitioned into binary categories as aquatic (including fully and semiaquatic) versus not aquatic, arboreal (or otherwise scansorial) versus not arboreal, and secretive (including fossorial, subfossorial, or leaf litter dwelling) versus not secretive. The aquatic and semiaquatic categories included those species that spend considerable portions of their adult lives in (and seeing through) water. Both a fully aquatic partition and a fully aquatic plus semiaquatic partition were tested. Arboreal (scansorial) species were those identified as having adaptations for climbing and/or spending considerable time in vegetation above the ground level. Secretive species included those active in the leaf litter or under other cover and those species active while burrowed in soil and sand. We also considered differences in geographic distribution and seasonality by partitioning tropical versus nontropical species, and considered differences in life history by partitioning metamorphosing species (i.e. including an aquatic tadpole phase with potentially different vision requirements than the adult phase) versus direct developers (lacking such tadpole phase). Trait scorings for the sampled species are illustrated in Fig. 2 and supplementary fig. S1, Supplementary Material online and are similar to those applied in Thomas et al. (2020, 2022b, 2022a). To score traits, we used peer-reviewed literature, online natural history resources, field guides, and field observations (supplementary file S1, Supplementary Material online).

Microspectrophotometry

While collecting eye samples for RNA-Seq, we collected the second eye from a subset of the species sampled for retinal microspectrophotometry (MSP) to estimate photoreceptor absorbance spectra. MSP methodology followed that described previously (Loew 1994; Loew et al. 2002; Schott et al. 2022a). Briefly, animals were dark adapted for at least 2 h and euthanized with MS-222. The eyes were enucleated under dim red light and hemisected, the retinas removed from the pigment epithelium under hypertonic buffer (pH 7.2 supplemented with 6%

sucrose), and pieces of retina were placed between two coverslips on the stage of a computer-controlled single-beam MSP (Loew 1994). Absorbance spectra were obtained for outer segments of multiple photoreceptor cell types from 350 to 750 nm with a wavelength accuracy of ~1 nm (Loew 1994). To estimate λ_{max} absorbance, data were fit to visual pigment templates using a standardized approach (Loew 1994; Schott et al. 2022a). Briefly, a Gaussian function was fit to the top 40 data points at 1 nm intervals and differentiated to establish the peak wavelength. The spectrum was normalized to the peak absorbance value and fit to either pure A_1 or A_2 chromophore templates from Govardovskii et al. (2000) following MacNichol (1986). Calculated absorbance values are accurate to ±1 nm.

Supplementary Material

Supplementary material is available at *Molecular Biology and Evolution* online.

Acknowledgments

Data Availability

The data underlying the study including transcriptome assemblies, sequence alignments, phylogenetic trees, and spectral-absorbance data are available in the Zenodo datasets (Schott et al. 2024a, 2024b). Sequence data were deposited in the NCBI under BioProject PRJNA1073881 (see supplementary file S1, Supplementary Material online for individual BioSample and SRA accession numbers).

References

Anderson SR, Wiens JJ. Out of the dark: 350 million years of conservatism and evolution in diel activity patterns in vertebrates. *Evolution*. 2017:**8**(8):1944–1959. https://doi.org/10.1111/evo.13284.

Anisimova M, Gascuel O. Approximate likelihood-ratio test for branches: a fast, accurate, and powerful alternative. *Syst Biol*. 2006:**55**(4):539–552. https://doi.org/10.1080/10635150600755453.

Asenjo AB, Rim J, Oprian DD. Molecular determinants of human red/green color discrimination. *Neuron*. 1994:**12**(5):1131–1138. https://doi.org/10.1016/0896-6273(94)90320-4.

Baker JL, Dunn KA, Mingrone J, Wood BA, Karpinski BA, Sherwood CC, Wildman DE, Maynard TM, Bielawski JP. Functional divergence of the nuclear receptor NR2C1 as a modulator of pluripotentiality during hominid evolution. *Genetics*. 2016:**203**(2):905–922. https://doi.org/10.1534/genetics.115.183889.

Batni S, Scalzetti L, Moody SA, Knox BE. Characterization of the *Xenopus* rhodopsin gene. *J Biol Chem*. 1996:**271**(6):3179–3186. https://doi.org/10.1074/jbc.271.6.3179.

Bickelmann C, Morrow JM, Muller J, Chang BSW. Functional characterization of the rod visual pigment of the echidna (Tachyglossus aculeatus), a basal mammal. *Vis Neurosci*. 2012:**29**(4-5):211–217. https://doi.org/10.1017/S0952523812000223.

Bielawski JP, Yang Z. A maximum likelihood method for detecting functional divergence at individual codon sites, with application to gene family evolution. *J Mol Evol*. 2004:**59**(1):121–132. https://doi.org/10.1007/s00239-004-2597-8.

Bloch NI, Morrow JM, Chang BSW, Price TD. SWS2 visual pigment evolution as a test of historically contingent patterns of plumage color evolution in warblers. *Evolution*. 2015:**69**(2):341–356. https://doi.org/10.1111/evo.12572.

Bolger AM, Lohse M, Usadel B. Trimmomatic: a flexible trimmer for Illumina sequence data. *Bioinformatics*. 2014:**30**(15):2114–2120. https://doi.org/10.1093/bioinformatics/btu170.

Bowmaker JK. Evolution of vertebrate visual pigments. *Vision Res*. 2008:**48**(20):2022–2041. https://doi.org/10.1016/j.visres.2008.03.025.

Boyette JL, Bell RC, Fujita MK, Thomas KN, Streicher JW, Gower DJ, Schott RK. Molecular evolution of non-visual opsin genes across environmental, developmental, and morphological adaptations in frogs. bioRxiv 515783. https://doi.org/10.1101/2022.11.10.515783, 14 November 2022, preprint: not peer reviewed.

Bridges CDB. The rhodopsin-porphyropsin visual system. In: Datnall HJA, editors. *Handbook of sensory Physiology VII/1: photochemistry of vision*. Berlin: Springer-Verlag; 1972. p. 417–480.

Carleton KL, Escobar-Camacho D, Stieb SM, Cortesi F, Marshall NJ. Seeing the rainbow: mechanisms underlying spectral sensitivity in teleost fishes. *J Exp Biol*. 2020:**223**(8):jeb193334. https://doi.org/10.1242/jeb.193334.

Carvalho LS, Pessoa DMA, Mountford JK, Davies WIL, Hunt DM. The genetic and evolutionary drives behind primate color vision. *Front Ecol Evol*. 2017:**5**:34. https://doi.org/10.3389/fevo.2017.00034.

Castiglione GM, Chang BS. Functional trade-offs and environmental variation shaped ancient trajectories in the evolution of dim-light vision. *Elife*. 2018:**7**:e35957. https://doi.org/10.7554/eLife.35957.

Castiglione GM, Chiu YLI, Gutierrez EA, Van Nynatten A, Hauser FE, Preston M, Bhattacharyya N, Schott RK, Chang BSW. Convergent evolution of dim light vision in owls and deep-diving whales. *Curr Biol*. 2023a:**33**(21):4733–4740.e4. https://doi.org/10.1016/j.cub.2023.09.015.

Castiglione GM, Hauser FE, Liao BS, Lujan NK, Van Nynatten A, Morrow JM, Schott RK, Bhattacharyya N, Dungan SZ, Chang BSW. Evolution of nonspectral rhodopsin function at high altitudes. *Proc Natl Acad Sci U S A*. 2017:**114**(28):7385–7390. https://doi.org/10.1073/pnas.1705765114.

Castiglione GM, Hauser FE, Van Nynatten A, Chang BSW. Adaptation of antarctic icefish vision to extreme environments. *Mol Biol Evol*. 2023b:**40**(4):msad030. https://doi.org/10.1093/molbev/msad030.

Chan T, Lee M, Sakmar TP. Introduction of hydroxyl-bearing amino acids causes bathochromic spectral shifts in rhodopsin. *J Biol Chem*. 1992:**267**(14):9478–9480. https://doi.org/10.1016/S0021-9258(19)50115-6.

Corredor VH, Hauzman E, da Silva Gonçalves A, Ventura DF. Genetic characterization of the visual pigments of the red-eared turtle (*Trachemys scripta elegans*) and computational predictions of the spectral sensitivity. *J Photochem Photobiol*. 2022:**12**:100141. https://doi.org/10.1016/j.jpap.2022.100141.

Cowing JA, Arrese CA, Davies WL, Beazley LD, Hunt DM. Cone visual pigments in two marsupial species: the fat-tailed dunnart (*Sminthopsis crassicaudata*) and the honey possum (*Tarsipes rostratus*). *Proc Biol Sci*. 2008:**275**(1642):1491–1499. https://doi.org/10.1098/rspb.2008.0248.

Cowing JA, Poopalasundaram S, Wilkie SE, Robinson PR, Bowmaker JK, Hunt DM. The molecular mechanism for the spectral shifts between vertebrate ultraviolet- and violet-sensitive cone visual pigments. *Biochem J*. 2002:**367**(1):129–135. https://doi.org/10.1042/bj20020483.

Cronin TW, Johnsen S, Marshall J, Warrant EJ. *Visual ecology*. Princeton: Princeton University Press; 2014.

Darden AG, Wu BX, Znoiko SL, Hazard ES, Kono M, Crouch RK, Ma JX. A novel *Xenopus* SWS2, P434 visual pigment: structure, cellular location, and spectral analyses. *Mol Vis*. 2003:**9**:191–199. http://www.molvis.org/molvis/v9/a28/.

Davies WIL, Collin SP, Hunt DM. Molecular ecology and adaptation of visual photopigments in craniates. *Mol Ecol*. 2012:**21**(13):3121–3158. https://doi.org/10.1111/j.1365-294X.2012.05617.x.

Delport W, Poon AFY, Frost SDW, Kosakovsky Pond SL. Datamonkey 2010: a suite of phylogenetic analysis tools for evolutionary biology. *Bioinforma Oxf Engl*. 2010:**26**(19):2455–2457. https://doi.org/10.1093/bioinformatics/btq429.

Donner K, Yovanovich CAM. A frog's eye view: foundational revelations and future promises. *Semin Cell Dev Biol*. 2020:**106**:72–85. https://doi.org/10.1016/j.semcdb.2020.05.011.

Duellman W, Trueb L. *Biology of amphibians*. Baltimore(MD): The Johns Hopkins University Press; 1994.

Dungan SZ, Chang BS. Epistatic interactions influence terrestrial–marine functional shifts in cetacean rhodopsin. *Proc R Soc B Biol Sci*. 2017:**284**(1850):20162743. https://doi.org/10.1098/rspb.2016.2743.

Dungan SZ, Kosyakov A, Chang BS. Spectral tuning of killer whale (*Orcinus orca*) rhodopsin: evidence for positive selection and functional adaptation in a cetacean visual pigment. *Mol Biol Evol*. 2016:**33**(2):323–336. https://doi.org/10.1093/molbev/msv217.

Edgar RC. MUSCLE: multiple sequence alignment with high accuracy and high throughput. *Nucleic Acids Res*. 2004:**32**(5):1792–1797. https://doi.org/10.1093/nar/gkh340.

Emerling CA, Springer MS. Eyes underground: regression of visual protein networks in subterranean mammals. *Mol Phylogenet Evol*. 2014:**78**:260–270. https://doi.org/10.1016/j.ympev.2014.05.016.

Enright JM, Toomey MB, Sato S, Temple SE, Allen JR, Fujiwara R, Kramlinger VM, Nagy LD, Johnson KM, Xiao Y, et al. Cyp27c1 red-shifts the spectral sensitivity of photoreceptors by converting vitamin A$_1$ into A$_2$. *Curr Biol*. 2015:**25**(23):3048–3057. https://doi.org/10.1016/j.cub.2015.10.018.

Feehan JM, Chiu CN, Stanar P, Tam BM, Ahmed SN, Moritz OL. Modeling dominant and recessive forms of retinitis pigmentosa by editing three rhodopsin-encoding genes in Xenopus laevis using Crispr/Cas9. *Sci. Rep*. 2017:**7**:6920.

Feng Y-J, Blackburn DC, Liang D, Hillis DM, Wake DB, Cannatella DC, Zhang P. Phylogenomics reveals rapid, simultaneous diversification of three major clades of Gondwanan frogs at the Cretaceous–Paleogene boundary. *Proc Natl Acad Sci U S A*. 2017:**114**(29):E5864. https://doi.org/10.1073/pnas.1704632114.

Fisher M, James-Zorn C, Ponferrada V, Bell AJ, Sundararaj N, Segerdell E, Chaturvedi P, Bayyari N, Chu S, Pells T, et al. Xenbase: key features and resources of the *Xenopus* model organism knowledgebase. *Genetics*. 2023:**224**(1):iyad018. https://doi.org/10.1093/genetics/iyad018.

Fortenbach CR, Kessler C, Peinado Allina G, Burns ME. Speeding rod recovery improves temporal resolution in the retina. *Vision Res*. 2015:**110**:57–67. https://doi.org/10.1016/j.visres.2015.02.011.

Gemmell NJ, Rutherford K, Prost S, Tollis M, Winter D, Macey JR, Adelson DL, Suh A, Bertozzi T, Grau JH, et al. The tuatara genome reveals ancient features of amniote evolution. *Nature*. 2020:**584**(7821):403–409. https://doi.org/10.1038/s41586-020-2561-9.

Govardovskii VI, Fyhrquist N, Reuter T, Kuzmin DG, Donner K. In search of the visual pigment template. *Vis Neurosci*. 2000:**17**(4):509–528. https://doi.org/10.1017/S0952523800174036.

Govardovskii VI, Reuter T. Why do green rods of frog and toad retinas look green? *J Comp Physiol A*. 2014:**200**(9):823–835. https://doi.org/10.1007/s00359-014-0925-z.

Gower DJ, Fleming JF, Pisani D, Vonk FJ, Kerkkamp HMI, Peichl L, Meimann S, Casewell NR, Henkel CV, Richardson MK, et al. Eye-transcriptome and genome-wide sequencing for scolecophidia: implications for inferring the visual system of the ancestral snake. *Genome Biol Evol*. 2021:**13**(12):evab253. https://doi.org/10.1093/gbe/evab253.

Grabherr MG, Haas BJ, Yassour M, Levin JZ, Thompson DA, Amit I, Adiconis X, Fan L, Raychowdhury R, Zeng Q, et al. Full-length transcriptome assembly from RNA-Seq data without a reference genome. *Nat Biotechnol*. 2011:**29**(7):644–652. https://doi.org/10.1038/nbt.1883.

Guindon S, Dufayard JF, Lefort V, Anisimova M, Hordijk W, Gascuel O. New algorithms and methods to estimate maximum-likelihood phylogenies: assessing the performance of PhyML 3.0. *Syst Biol*. 2010:**59**(3):307–321. https://doi.org/10.1093/sysbio/syq010.

Gutierrez EA, Castiglione GM, Morrow JM, Schott RK, Loureiro LO, Lim BK, Chang BSW. Functional shifts in bat dim-light visual pigment are associated with differing echolocation abilities and reveal molecular adaptation to photic-limited environments. *Mol Biol Evol*. 2018a:**35**(10):2422–2434. https://doi.org/10.1093/molbev/msy140.

Gutierrez EA, Schott RK, Preston MW, Loureiro LO, Lim BK, Chang BSW. The role of ecological factors in shaping bat cone opsin

evolution. *Proc Biol Sci*. 2018b:**285**(1876):20172835. https://doi.org/10.1098/rspb.2017.2835.

Hagen JFD, Roberts NS, Johnston RJ. The evolutionary history and spectral tuning of vertebrate visual opsins. *Dev Biol*. 2023:**493**: 40–66. https://doi.org/10.1016/j.ydbio.2022.10.014.

Hárosi FI. Recent results from single-cell microspectrophotometry: cone pigments in frog, fish, and monkey. *Color Res Appl*. 1982:**7**(2):135–141. https://doi.org/10.1002/col.5080070216.

Hart NS, Bailes HJ, Vorobyev M, Marshall NJ, Collin SP. Visual ecology of the Australian lungfish (*Neoceratodus forsteri*). *BMC Ecol*. 2008:**8**(1):21. https://doi.org/10.1186/1472-6785-8-21.

Hauser FE, Ilves KL, Schott RK, Alvi E, López-Fernández H, Chang BSW. Evolution, inactivation and loss of short wavelength-sensitive opsin genes during the diversification of Neotropical cichlids. *Mol Ecol*. 2021:**30**(7):1688–1703. https://doi.org/10.1111/mec.15838.

Hauser FE, Ilves KL, Schott RK, Castiglione GM, Lopez-Fernandez H, Chang BSW. Accelerated evolution and functional divergence of the dim light visual pigment accompanies cichlid colonization of Central America. *Mol Biol Evol*. 2017:**34**(10):2650–2664. https://doi.org/10.1093/molbev/msx192.

Hauzman E, Bonci DMO, Suárez-Villota EY, Neitz M, Ventura DF. Daily activity patterns influence retinal morphology, signatures of selection, and spectral tuning of opsin genes in colubrid snakes. *BMC Evol Biol*. 2017:**17**(1):249. https://doi.org/10.1186/s12862-017-1110-0.

Hauzman E, Pierotti MER, Bhattacharyya N, Tashiro JH, Yovanovich CAM, Campos PF, Ventura DF, Chang BSW. Simultaneous expression of UV and violet SWS1 opsins expands the visual palette in a group of freshwater snakes. *Mol Biol Evol*. 2021:**38**(12): 5225–5240. https://doi.org/10.1093/molbev/msab285.

Hisatomi O, Kayada S, Taniguchi Y, Kobayashi Y, Satoh T, Tokunaga F. Primary structure and characterization of a bullfrog visual pigment contained in small single cones. *Comp Biochem Physiol B Biochem Mol Biol*. 1998:**119**(3):585–591. https://doi.org/10.1016/S0305-0491(98)00032-7.

Hisatomi O, Takahashi Y, Taniguchi Y, Tsukahara Y, Tokunaga F. Primary structure of a visual pigment in bullfrog green rods. *FEBS Lett*. 1999:**447**(1):44–48. https://doi.org/10.1016/S0014-5793(99)00209-4.

Hödl W, Amézquita A. Visual signaling in anuran amphibians. In: Ryan MJ, editor. *Anuran communication*. Washington: Smithsonian Institution Press; 2001. p. 121–141.

Hunt DM, Dulai KS, Partridge JC, Cottrill P, Bowmaker JK. The molecular basis for spectral tuning of rod visual pigments in deep-sea fish. *J Exp Biol*. 2001:**204**:3333–3344. https://doi.org/10.1242/jeb.204.19.3333.

Ingle D. Behavioral correlates of central visual function in anurans. In: Llinás R, Precht W, editors. *Frog neurobiology: a handbook*. Berlin: Springer Berlin Heidelberg; 1976. p. 435–451.

Isayama T, Chen Y, Kono M, Fabre E, Slavsky M, DeGrip WJ, Ma JX, Crouch RK, Makino CL. Coexpression of three opsins in cone photoreceptors of the salamander *Ambystoma tigrinum*. *J Comp Neurol*. 2014:**522**(10):2249–2265. https://doi.org/10.1002/cne.23531.

Isayama T, Makino C. Pigment mixtures and other determinants of spectral sensitivity of vertebrate retinal photoreceptors. In: Akutagawa E Ozaki K, editors. *Photoreceptors Physiol Types Abnorm*. Hauppauge: Nova Science; 2012. p. 1–31.

Jetz W, Pyron RA. The interplay of past diversification and evolutionary isolation with present imperilment across the amphibian tree of life. *Nat Ecol Evol*. 2018:**2**(5):850–858. https://doi.org/10.1038/s41559-018-0515-5.

King R, Douglass J, Phillips J, Baube C. Scotopic spectral sensitivity of the optomotor response in the green tree frog *Hyla cinerea*. *J Exp Zool*. 1993:**267**(1):40–46. https://doi.org/10.1002/jez.1402670107.

Kojima K, Matsutani Y, Yamashita T, Yanagawa M, Imamoto Y, Yamano Y, Wada A, Hisatomi O, Nishikawa K, Sakurai K, *et al*. Adaptation of cone pigments found in green rods for scotopic vision through a single amino acid mutation. *Proc Natl Acad Sci U S A*. 2017:**114**(21):5437–5442. https://doi.org/10.1073/pnas.1620010114.

Korenyak DA, Govardovskii VI. Photoreceptors and visual pigments in three species of newts. *J Evol Biochem Physiol*. 2013:**49**(4): 399–407. https://doi.org/10.1134/S0022093013040038.

Kosakovsky Pond SL, Murrell B, Fourment M, Frost SDW, Delport W, Scheffler K. A random effects branch-site model for detecting episodic diversifying selection. *Mol Biol Evol*. 2011:**28**(11): 3033–3043. https://doi.org/10.1093/molbev/msr125.

Koskelainen A, Hemilä S, Donner K. Spectral sensitivities of short- and long-wavelength sensitive cone mechanisms in the frog retina. *Acta Physiol Scand*. 1994:**152**(1):115–124. https://doi.org/10.1111/j.1748-1716.1994.tb09790.x.

Lamb TD, Patel H, Chuah A, Natoli RC, Davies WI, Hart NS, Collin SP, Hunt DM. Evolution of vertebrate phototransduction: cascade activation. *Mol Biol Evol*. 2016:**33**(8):2064–2087. https://doi.org/10.1093/molbev/msw095.

Land MF, Nilsson DE. Lens eyes on land. In: Land MF, Nilsson DE, editors. *Animal eyes*. Oxford: Oxford University Press; 2012. p. 94–129.

Li H, 2013. Aligning sequence reads, clone sequences and assembly contigs with BWA-MEM. arXiv, arXiv:1303.3997v1, preprint: not peer reviewed.

Liebman PA. Microspectrophotometry of photoreceptors. In: Dartnall HJA, editor. *Photochemistry of vision*. Berlin: Springer Berlin Heidelberg; 1972. p. 481–528.

Liebman PA, Entine G. Visual pigments of frog and tadpole (*Rana pipiens*). *Vision Res*. 1968:**8**(7):761–775. https://doi.org/10.1016/0042-6989(68)90128-4.

Loew ER. A third, ultraviolet-sensitive, visual pigment in the Tokay gecko (*Gekko gekko*). *Vision Res*. 1994:**34**(11):1427–1431. https://doi.org/10.1016/0042-6989(94)90143-0.

Loew ER, Fleishman LJ, Foster RG, Provencio I. Visual pigments and oil droplets in diurnal lizards: a comparative study of Caribbean anoles. *J Exp Biol*. 2002:**205**(7):927–938. https://doi.org/10.1242/jeb.205.7.927.

Lupše N, Cortesi F, Freese M, Marohn L, Pohlmann J-D, Wysujack K, Hanel R, Musilova Z. Visual gene expression reveals a cone-to-rod developmental progression in deep-sea fishes. *Mol Biol Evol*. 2021:**38**(12):5664–5677. https://doi.org/10.1093/molbev/msab281.

Ma JX, Znoiko S, Othersen KL, Ryan JC, Das J, Isayama T, Kono M, Oprian DD, Corson DW, Cornwall MC, *et al*. A visual pigment expressed in both rod and cone photoreceptors. *Neuron*. 2001:**32**(3): 451–461. https://doi.org/10.1016/S0896-6273(01)00482-2.

MacNichol EF. A unifying presentation of photopigment spectra. *Vision Res*. 1986:**26**(9):1543–1556. https://doi.org/10.1016/0042-6989(86)90174-4.

Martin M. CUTADAPT removes adapter sequences from high-throughput sequencing reads. *EMBnet J*. 2011:**17**(1):10. https://doi.org/10.14806/ej.17.1.200.

McDevitt DS, Brahma SK, Jeanny JC, Hicks D. Presence and foveal enrichment of rod opsin in the all-cone retina of the American chameleon. *Anat Rec*. 1993:**237**(3):299–307. https://doi.org/10.1002/ar.1092370302.

Mège P, Ödeen A, Théry M, Picard D, Secondi J. Partial opsin sequences suggest UV-sensitive vision is widespread in Caudata. *Evol Biol*. 2016:**43**(1):109–118. https://doi.org/10.1007/s11692-015-9353-4.

Meredith RW, Gatesy J, Emerling CA, York VM, Springer MS. Rod monochromacy and the coevolution of cetacean retinal opsins. *PLoS Genet*. 2013:**9**(4):e1003432. https://doi.org/10.1371/journal.pgen.1003432.

Mitra AT, Womack MC, Gower DJ, Streicher JW, Clark B, Bell RC, Schott RK, Fujita MK, Thomas KN. Ocular lens morphology is influenced by ecology and metamorphosis in frogs and toads. *Proc R Soc B Biol Sci*. 2022:**289**(1987):20220767. https://doi.org/10.1098/rspb.2022.0767.

Mohun SM, Davies WL, Bowmaker JK, Pisani D, Himstedt W, Gower DJ, Hunt DM, Wilkinson M. Identification and characterization of visual pigments in caecilians (Amphibia: gymnophiona), an

order of limbless vertebrates with rudimentary eyes. *J Exp Biol*. 2010:213(20):3586–3592. https://doi.org/10.1242/jeb.045914.

Mulhair PO, Crowley L, Boyes DH, Lewis OT, Holland PWH. Opsin gene duplication in lepidoptera: retrotransposition, sex linkage, and gene expression. *Mol Biol Evol*. 2023:40(11):msad241. https://doi.org/10.1093/molbev/msad241.

Murrell B, Moola S, Mabona A, Weighill T, Sheward D, Kosakovsky Pond SL, Scheffler K. FUBAR: a fast, unconstrained Bayesian AppRoximation for inferring selection. *Mol Biol Evol*. 2013:30(5):1196–1205. https://doi.org/10.1093/molbev/mst030.

Murrell B, Weaver S, Smith MD, Wertheim JO, Murrell S, Aylward A, Eren K, Pollner T, Martin DP, Smith DM, et al. Gene-wide identification of episodic selection. *Mol Biol Evol*. 2015:32(5):1365–1371. https://doi.org/10.1093/molbev/msv035.

Musilova Z, Salzburger W, Cortesi F. The visual opsin gene repertoires of teleost fishes: evolution, ecology, and function. *Annu Rev Cell Dev Biol*. 2021:37(1):441–468. https://doi.org/10.1146/annurev-cellbio-120219-024915.

Partha R, Chauhan BK, Ferreira Z, Robinson JD, Lathrop K, Nischal KK, Chikina M, Clark NL. Subterranean mammals show convergent regression in ocular genes and enhancers, along with adaptation to tunneling. *Elife*. 2017:6:e25884. https://doi.org/10.7554/eLife.25884.

Peinado Allina G, Fortenbach C, Naarendorp F, Gross OP, Pugh EN Jr, Burns ME. Bright flash response recovery of mammalian rods in vivo is rate limited by RGS9. *J Gen Physiol*. 2017:149(4):443–454. https://doi.org/10.1085/jgp.201611692.

Pond SLK, Frost SDW. A genetic algorithm approach to detecting lineage-specific variation in selection pressure. *Mol Biol Evol*. 2005:22(3):478–485. https://doi.org/10.1093/molbev/msi031.

Pyron RA, Wiens JJ. A large-scale phylogeny of amphibia including over 2800 species, and a revised classification of extant frogs, salamanders, and caecilians. *Mol Phylogenet Evol*. 2011:61(2):543–583. https://doi.org/10.1016/j.ympev.2011.06.012.

Robertson JM, Bell RC, Loew ER. Vision in dim light and the evolution of color pattern in a crepuscular/nocturnal frog. *Evol Ecol*. 2022:36(3):355–371. https://doi.org/10.1007/s10682-022-10173-w.

Rogers RL, Zhou L, Chu C, Márquez R, Corl A, Linderoth T, Freeborn L, MacManes MD, Xiong Z, Zheng J, et al. Genomic takeover by transposable elements in the strawberry poison frog. *Mol Biol Evol*. 2018:35(12):2913–2927. https://doi.org/10.1093/molbev/msy185.

Rossetto IH, Sanders KL, Simões BF, Van Cao N, Ludington AJ. Functional duplication of the short-wavelength-sensitive opsin in sea snakes: evidence for reexpanded color sensitivity following ancestral regression. *Genome Biol Evol*. 2023:15(7):evad107. https://doi.org/10.1093/gbe/evad107.

Schott RK, Bell RC, Loew ER, Thomas KN, Gower DJ, Streicher JW, Fujita MK. Transcriptomic evidence for visual adaptation during the aquatic to terrestrial metamorphosis in leopard frogs. *BMC Biol*. 2022a:20(1):138. https://doi.org/10.1186/s12915-022-01341-z.

Schott RK, Bhattacharyya N, Chang BSW. Evolutionary signatures of photoreceptor transmutation in geckos reveal potential adaptation and convergence with snakes. *Evolution*. 2019:73(9):1958–1971. https://doi.org/10.1111/evo.13810.

Schott RK, Fujita MK, Streicher JW, Gower DJ, Thomas KN, Ellis L, Bamba Kaya A, Bittencourt-Silva G, Becker CG, Cisneros-Heredia D, et al. Data from: Diversity and evolution of frog visual opsins: spectral tuning and adaptation to distinct light environments [Data set]. *Zenodo*. 2024a. https://doi.org/10.5281/zenodo.10622170.

Schott RK, Fujita MK, Streicher JW, Gower DJ, Thomas KN, Bell RC. Frog Eye Transcriptome Assemblies [Data set]. *Zenodo*. 2024b. https://doi.org/10.5281/zenodo.10620583.

Schott RK, Muller J, Yang CG, Bhattacharyya N, Chan N, Xu M, Morrow JM, Ghenu AH, Loew ER, Tropepe V, et al. Evolutionary transformation of rod photoreceptors in the all-cone retina of a diurnal garter snake. *Proc Natl Acad Sci U S A*. 2016:113(2):356–361. https://doi.org/10.1073/pnas.1513284113.

Schott RK, Panesar B, Card DC, Preston M, Castoe TA, Chang BS. Targeted capture of complete coding regions across divergent species. *Genome Biol Evol*. 2017:9(2):398–414. https://doi.org/10.1093/gbe/evx005.

Schott RK, Perez L, Kwiatkowski MA, Imhoff V, Gumm JM. Evolutionary analyses of visual opsin genes in frogs and toads: diversity, duplication, and positive selection. *Ecol Evol*. 2022b:12(2):e8595. https://doi.org/10.1002/ece3.8595.

Schott RK, Refvik SP, Hauser FE, Lopez-Fernandez H, Chang BS. Divergent positive selection in rhodopsin from lake and riverine cichlid fishes. *Mol Biol Evol*. 2014:31(5):1149–1165. https://doi.org/10.1093/molbev/msu064.

Schott RK, Van Nynatten A, Card DC, Castoe TA, S. W. Chang B. Shifts in selective pressures on snake phototransduction genes associated with photoreceptor transmutation and dim-light ancestry. *Mol Biol Evol*. 2018:35(6):1376–1389. https://doi.org/10.1093/molbev/msy025.

Session AM, Uno Y, Kwon T, Chapman JA, Toyoda A, Takahashi S, Fukui A, Hikosaka A, Suzuki A, Kondo M, et al. Genome evolution in the allotetraploid frog *Xenopus laevis*. *Nature*. 2016:538(7625):336–343. https://doi.org/10.1038/nature19840.

Siddiqi A, Cronin TW, Loew ER, Vorobyev M, Summers K. Interspecific and intraspecific views of color signals in the strawberry poison frog *Dendrobates pumilio*. *J Exp Biol*. 2004:207(14):2471–2485. https://doi.org/10.1242/jeb.01047.

Simões BF, Sampaio FL, Douglas RH, Kodandaramaiah U, Casewell NR, Harrison RA, Hart NS, Partridge JC, Hunt DM, Gower DJ. Visual pigments, ocular filters and the evolution of snake vision. *Mol Biol Evol*. 2016:33(10):2483–2495. https://doi.org/10.1093/molbev/msw148.

Starace DM, Knox BE. Cloning and expression of a *Xenopus* short wavelength cone pigment. *Exp Eye Res*. 1998:67(2):209–220. https://doi.org/10.1006/exer.1998.0507.

Streicher JW, Miller EC, Guerrero PC, Correa C, Ortiz JC, Crawford AJ, Pie MR, Wiens JJ. Evaluating methods for phylogenomic analyses, and a new phylogeny for a major frog clade (Hyloidea) based on 2214 loci. *Mol Phylogenet Evol*. 2018:119:128–143. https://doi.org/10.1016/j.ympev.2017.10.013.

Stuckert AMM, Chouteau M, McClure M, LaPolice TM, Linderoth T, Nielsen R, Summers K, MacManes MD. The genomics of mimicry: gene expression throughout development provides insights into convergent and divergent phenotypes in a Müllerian mimicry system. *Mol Ecol*. 2021:30(16):4039–4061. https://doi.org/10.1111/mec.16024.

Sugawara T, Imai H, Nikaido M, Imamoto Y, Okada N. Vertebrate rhodopsin adaptation to dim light via rapid meta-II intermediate formation. *Mol Biol Evol*. 2010:27(3):506–519. https://doi.org/10.1093/molbev/msp252.

Takahashi Y, Hisatomi O, Sakakibara S, Tokunaga F, Tsukahara Y. Distribution of blue-sensitive photoreceptors in amphibian retinas. *FEBS Lett*. 2001:501(2-3):151–155. https://doi.org/10.1016/S0014-5793(01)02632-1.

Takahashi Y, Yokoyama S. Genetic basis of spectral yuning in the violet-sensitive visual pigment of African clawed frog, *Xenopus laevis*. *Genetics*. 2005:171(3):1153–1160. https://doi.org/10.1534/genetics.105.045849.

Tamura K, Peterson D, Peterson N, Stecher G, Nei M, Kumar S. MEGA5: molecular evolutionary genetics analysis using maximum likelihood, evolutionary distance, and maximum parsimony methods. *Mol Biol Evol*. 2011:28(10):2731–2739. https://doi.org/10.1093/molbev/msr121.

Thomas KN, Gower DJ, Bell RC, Fujita MK, Schott RK, Streicher JW. Eye size and investment in frogs and toads correlate with adult habitat, activity pattern and breeding ecology. *Proc R Soc B Biol Sci*. 2020:287(1935):20201393. https://doi.org/10.1098/rspb.2020.1393.

Thomas KN, Gower DJ, Streicher JW, Bell RC, Fujita MK, Schott RK, Liedtke HC, Haddad CFB, Becker CG, Cox CL, et al. Ecology drives patterns of spectral transmission in the ocular lenses of frogs and salamanders. *Funct Ecol*. 2022a:36(4):850–864. https://doi.org/10.1111/1365-2435.14018.

Thomas KN, Rich C, Quock RC, Streicher JW, Gower DJ, Schott RK, Fujita MK, Douglas RH, Bell RC. Diversity and evolution of amphibian pupil shapes. *Biol J Linn Soc*. 2022b:**137**(3):434–449. https://doi.org/10.1093/biolinnean/blac095.

Torres-Dowdall J, Henning F, Elmer KR, Meyer A. Ecological and lineage-specific factors drive the molecular evolution of rhodopsin in cichlid fishes. *Mol Biol Evol*. 2015:**32**(11):2876–2882. https://doi.org/10.1093/molbev/msv159.

Van Nynatten A, Castiglione GM, de A Gutierrez E, Lovejoy NR, Chang BSW. Recreated ancestral opsin associated with marine to freshwater croaker invasion reveals kinetic and spectral adaptation. *Mol Biol Evol*. 2021:**38**(5):2076–2087. https://doi.org/10.1093/molbev/msab008.

Veilleux CC, Louis EE, Bolnick DA. Nocturnal light environments influence color vision and signatures of selection on the OPN1SW opsin gene in nocturnal lemurs. *Mol Biol Evol*. 2013:**30**(6):1420–1437. https://doi.org/10.1093/molbev/mst058.

Wan YC, Navarrete Méndez MJ, O'Connell LA, Uricchio LH, Roland A-B, Maan ME, Ron SR, Betancourth-Cundar M, Pie MR, Howell KA, *et al*. Selection on visual opsin genes in diurnal neotropical frogs and loss of the sws2 opsin in poison frogs. *Mol Biol Evol*. 2023:**40**(10):msad206. https://doi.org/10.1093/molbev/msad206.

Weadick CJ, Chang BSW. An improved likelihood ratio test for detecting site-specific functional divergence among clades of protein-coding genes. *Mol Biol Evol*. 2012:**29**(5):1297–1300. https://doi.org/10.1093/molbev/msr311.

Wertheim JO, Murrell B, Smith MD, Kosakovsky Pond SL, Scheffler K. RELAX: detecting relaxed selection in a phylogenetic framework. *Mol Biol Evol*. 2015:**32**(3):820–832. https://doi.org/10.1093/molbev/msu400.

Witkovsky P, Levine JS, Engbretson GA, Hassin G, MacNichol EF. A microspectrophotometric study of normal and artificial visual pigments in the photoreceptors of *Xenopus laevis*. *Vision Res*. 1981:**21**(6):867–873. https://doi.org/10.1016/0042-6989(81)90187-5.

Wu Y, Hadly EA, Teng W, Hao Y, Liang W, Liu Y, Wang H. Retinal transcriptome sequencing sheds light on the adaptation to nocturnal and diurnal lifestyles in raptors. *Sci Rep*. 2016:**6**(1):33578. https://doi.org/10.1038/srep33578.

Xu P, Lu B, Chao J, Holdbrook R, Liang G, Lu Y. The evolution of opsin genes in five species of mirid bugs: duplication of long-wavelength opsins and loss of blue-sensitive opsins. *BMC Ecol Evol*. 2021:**21**(1):66. https://doi.org/10.1186/s12862-021-01799-5.

Yang Z. PAML 4: phylogenetic analysis by maximum likelihood. *Mol Biol Evol*. 2007:**24**(8):1586–1591. https://doi.org/10.1093/molbev/msm088.

Yokoyama S. Evolution of dim-light and color vision pigments. *Annu Rev Genomics Hum Genet*. 2008:**9**(1):259–282. https://doi.org/10.1146/annurev.genom.9.081307.164228.

Yokoyama S, Shi Y. Genetics and evolution of ultraviolet vision in vertebrates. *FEBS Lett*. 2000:**486**(2):167–172. https://doi.org/10.1016/S0014-5793(00)02269-9.

Yokoyama S, Tada T, Zhang H, Britt L. Elucidation of phenotypic adaptations: molecular analyses of dim-light vision proteins in vertebrates. *Proc Natl Acad Sci U S A*. 2008:**105**(36):13480–13485. https://doi.org/10.1073/pnas.0802426105.

Yokoyama S, Takenaka N, Agnew DW, Shoshani J. Elephants and human color-blind deuteranopes have identical sets of visual pigments. *Genetics*. 2005:**170**(1):335–344. https://doi.org/10.1534/genetics.104.039511.

Yokoyama S, Takenaka N, Blow N. A novel spectral tuning in the short wavelength-sensitive (SWS1 and SWS2) pigments of bluefin killifish (*Lucania goodei*). *Gene*. 2007:**396**(1):196–202. https://doi.org/10.1016/j.gene.2007.03.019.

Yovanovich CAM, Grant T, Kelber A. Differences in ocular media transmittance in classical frog and toad model species and its impact on visual sensitivity. *J Exp Biol*. 2019:**222**:jeb204271. https://doi.org/10.1242/jeb.204271.

Yovanovich CAM, Pierotti MER, Kelber A, Jorgewich-Cohen G, Ibáñez R, Grant T. Lens transmittance shapes ultraviolet sensitivity in the eyes of frogs from diverse ecological and phylogenetic backgrounds. *Proc R Soc B Biol Sci*. 2020:**287**(1918):20192253. https://doi.org/10.1098/rspb.2019.2253.